

Referee 1

Dear Editor,

5 ***We first would like to thank the reviewer for all the remarks and suggestions very useful to improve the manuscript. We have tried to take into account most of the mentioned following points.***

10 This is a well written and straightforward paper on model simulations of heating rates compared to and at times constrained by the ORACLES and LASIC field campaigns. I found it easy to read and well laid out. They take a best available run with the model, and clearly spell out modeled radiative, temperature and PBL effects. They note biases and deficiencies, particularly in reference to wind and smoke vertical profile.

15 I have a few minor comments (listed below) but one major comment. I would like to direct the authors to Tom Ecks paper <https://agupubs.onlinelibrary.wiley.com/doi/full/10.1002/jgrd.50500> on the seasonal trends of wind over Africa. One thing the paper failed to account for is that wind over Africa has a very strong and very predictable trend due to a systematic shift in grass burning in the early season to more wooded fire late in the season, roughly 0.83 in early July, to 0.92 in mid-October at 440 nm. Yet, the real part of the index of refraction and the size distribution remain relatively static. This makes for an outstanding natural partial derivative on the sensitivity of the system to black carbon. However in the paper the black carbon mass fraction is static for the burning season. While I do not think that they necessarily need to do another run (as the model simulation is for the middle 2 months and results are largely aggregated), I think that at least a paragraph or two needs to be present adding context to their run and providing rough error estimates, sensitivity and implication (if any) of this strong seasonal trend. In particular, please compare this finding to what you found in the model (Line 618).

20 I have lots minor comments that I think might clarify the paper. Some of this is because it is just the way the model was constructed and the investigators are sort of stuck with it. I don't mind so much of their assumed parameters are out of expected range by a little bit, but it should probably be noted. Also, things that seem minor information is actually very helpful later on when people try to reconcile model runs and observations. So please do your best to address these

25 ***We agree on this important limitation concerning the representation of smoke optical properties (notably absorption) in the ALADIN-Climate model. As fires are not explicitly resolved in the model, it is difficult to take into account changes in optical properties of smoke during the biomass burning season. In that sense, we have only investigated here the August-September period when smoke SSA remains low, around 0.84-0.86 at 500nm (AERONET retrievals ; Eck et al., 2013). In addition, this ALADIN-Climate simulation has been also constrained by recent in-situ observations (Zuidema et al., 2018) obtained within the marine boundary layer at Ascension island (SSA of ~0.80 at 550 nm in September 2016). Anyway, it is clear that this hypothesis is important and could have some implications on biomass burning shortwave (SW) heating rate and direct radiative effect especially for climate simulations including all the biomass burning season (from July to late October).***

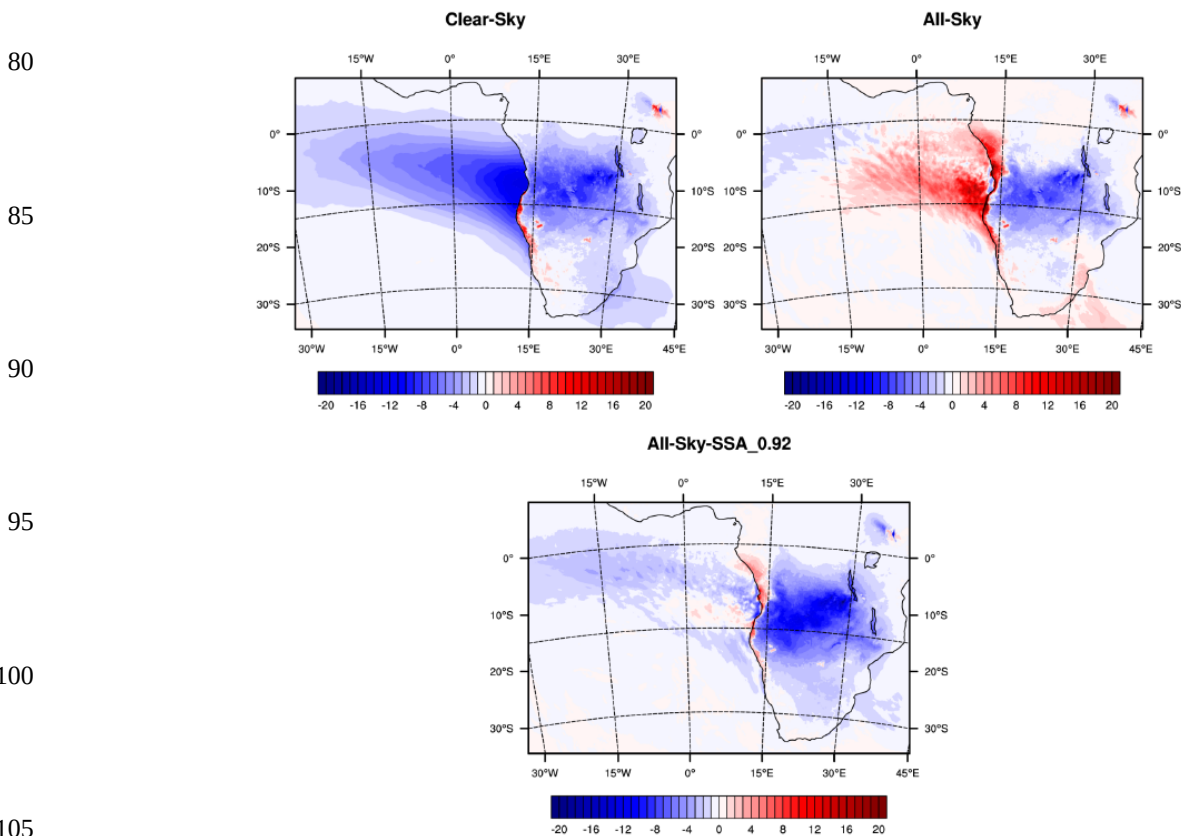
35 ***To address this specific point, we have now performed a new simulation, named SMK_SSA, which includes less absorbing smoke, more representative of the late season (September-October) as noted by Eck et al. (2013). In this sensitivity simulation, SSA has been fixed to 0.92 (550 nm) for smoke; the rest of BBA parameters being exactly similar. The description of this new simulation is now included in the paragraph 3.1 and this limitation of the ALADIN-Climate model is clearly reminded in the part 2.2. To illustrate these new results, the figure 13 has been modified (see the new Figure 13 below) and a new Table (Table 3) has been included.***

45 ***Along the text, additional explanations are now provided in terms of sensitivity on (i) SW heating rate (paragraph 4.2.4.3), (ii) direct radiative effect exerted at the top of the atmosphere and (iii) the different impacts on surface SW radiations, temperature, sensible heat fluxes and PBL height.***

50 ***In terms of SW radiative heating and direct radiative forcing, this new ALADIN simulation indicates :***

- 60 - a significant decrease of the SW radiative heating induced by smoke. For example and over the Box_S (defined over the sources of biomass burning), SW heating at 3km is passing from +1.15°K by day to +0.58°K by day. This point could moderate the heating induced by smoke at the end of the biomass burning season. This point is now included in the article (paragraph 4.2.4.3),
- 65 - a significant change in the monthly-mean (September 2016) DRF at TOA, passing from a positive (+4.2 W.m⁻²) to negative (-0.54 W.m⁻²) direct forcing (see new Figure 13 and Table 3) over the Box_O (ocean). This means that the positive direct forcing at TOA could be lesser in intensity at the end of the BBA season (late october). This important point is now mentioned in the part 5.1 and the results of the new ALADIN-Climate (SMK_SSA) simulation with more scattering smoke (SSA of 0.92) are included in the Table 3,
- 70 - a more intense negative DRF at TOA over smoke sources due to more scattering BBA. Over the box_S, the monthly-mean value DRF is increasing from -3.9 W.m⁻² (SMK) to -7.3 W.m⁻² (SMK_SSA). This specific point is added in the discussion. Values are reported in the Table 3,
- 75 - a less important positive DRF is observed at TOA along the Southern African coast and Gabon due to more scattering BBA. This important point is now indicated in the paragraph 5.1,

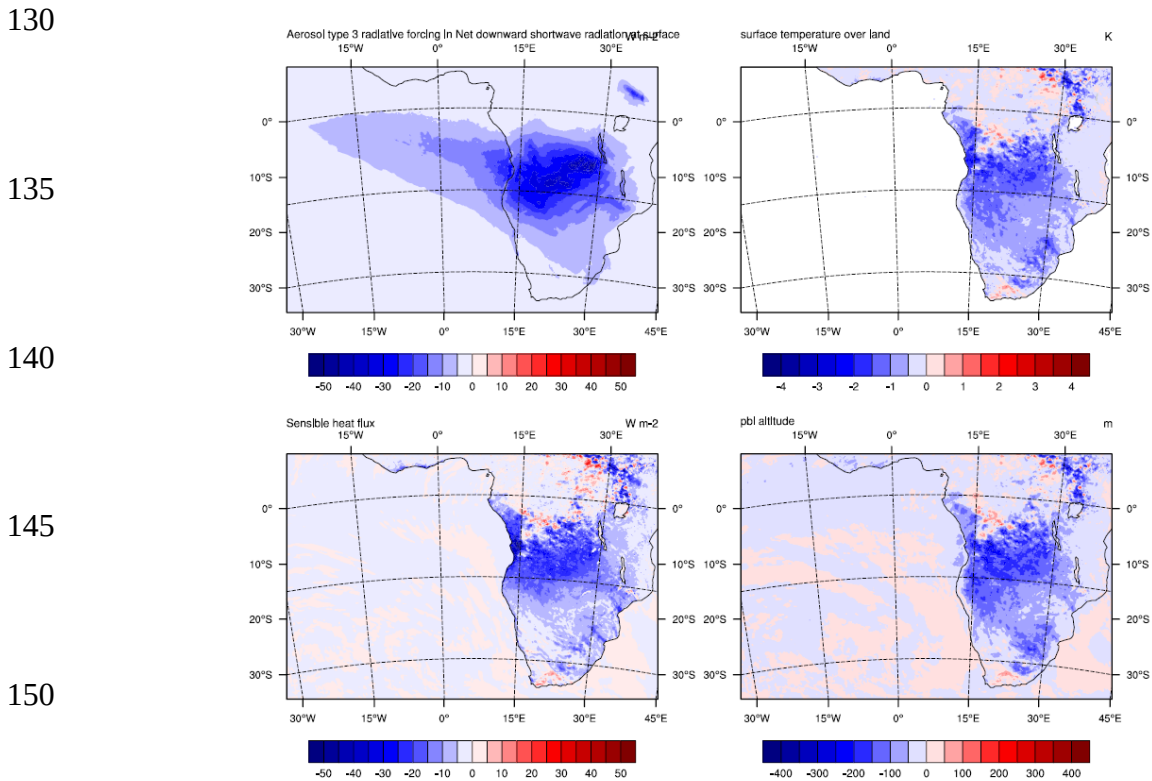
ALADIN-Climat Monthly-mean DRF (SW) at TOA - September 2016



110 *New figure 13 including (bottom) the monthly-mean DRF exerted at TOA for more scattering smoke (SMK_SSA simulation).*

115 *Concerning the impact of BBA on other variables (SW radiations at the surface, surface temperature, sensible heat fluxes and PBL height), we did exactly the same figure as Figure 14 but for the new simulation (SSA_SMK). This new figure (see below) has been added in Supplement material (S8) and the main results are discussed in the Part 5.2. We have notably added these clarifications :*

120 «Finally, the comparisons with the SMK_SSA simulations (not shown, Figure S8) indicate a decrease of
 the surface radiative forcing both over continent and ocean. As reported in Table 3, the monthly-mean
 DRF at BOA is about -39 W.m^{-2} and -25 W.m^{-2} over Box_S (biomasse burning sources) for the SMK and
 SMK_SSA simulations, respectively. The same result is obtained over SAO. This is due to the decrease of
 125 SW radiations absorbed by smoke in the SMK_SSA simulation, increasing the SW radiations reaching the
 surface. This could be also due, to a lesser extent, to some changes in aerosol loading due to
 modifications in the dynamics and precipitation between the two simulations. This induces a less
 pronounced impact of BBA on the surface temperature and sensible heat fluxes in the SMK_SSA run.
 130 The increase of SW surface radiations, associated to low absorption by BBA in SMK_SSA, decrease the
 impact of smoke on the PBL development (Figure S8). As mentioned previously, these results suggest that
 the impact of BBA on the surface fluxes and dynamics are certainly slightly lower at the end of the
 biomass burning season.»



155 **The new Figure S7, which is now included in the supplement material.**

Line 79: the first few times please state warming/cooling in association with positive and negative DRF for clarity for readers

This point is now included in the new version.

160

Line 163. The use of OC/BC as biomass burning tracer with fixed microphysical and optical properties and basically being in the same emission category with anthropogenic is somewhat problematic and their hypothesis ‘implications’ are almost certainly violated in the study regime, especially on the northern end of the core biomass burning feature. This is a recurring problem in the modeling community, and has led to significant discussion within the ICAP community. The bottom line is that carbonations species are fundamentally different from biomass burning and anthropogenic/biogenic sources, and should be treated separately in models. But, model architecture is not so easy to change. I think the authors need to be clear about this up front and add a few lines discussing specifically what this does to the simulation. Fortunately for them, biomass burning particle evolution tends to be rather fast, slowing down by the time it reaches the coastline (<https://www.atmos-chem-phys.net/5/799/2005/>). This said, however, African smoke

165

170

has shown evidence of evaporation/sublimation as noted in <https://link.springer.com/article/10.1007/BF00708178>.

175 ***We agree with this remark, which represents one of the main motivations for including two new specific tracers in the ALADIN-Climate model to represent BBA, as presented in the part 2.2. This allows now to take into account specific properties for smoke particles, as the hygroscopic, e-folding time and optical properties. It allows notably to distinguish those particles from carbonaceous aerosols emitted from anthropogenic emissions with different properties. This point is now more detailed in the text (part 2.2).***

180 Line 171. Again, based on lit review <https://www.atmos-chem-phys.net/5/799/2005/> is more in line with Vakkari. It is complicated because one has to decide what the initial state is to start the clock ticking. There is substantial evidence of difference in smoke properties from the base and top of a smoke column too. I think this is fairly moot though given the large scale nature of the simulation.

185 ***This is right, and the reason why we had performed an additional simulation using a different e-folding time (provided in the Appendix; Figure S1). We show that using a value of 3 hours (Vakkari et al., 2018) leads to change in AOD of about ~0.05 over the biomass burning region. This suggests, for this specific case, a modest impact on AOD compared to the hypothesis made on the POM to OC ratio. This point is indicated in the part 3.1 and deeper discussed in the new version.***

190 Line 188. Just an FYI, you should note that these values of MEE are just on the upper half of what has been gravimetrically observed <https://www.atmos-chem-phys.net/5/827/2005/acp-5-827-2005.pdf> But 5 is a nice round number.

Thank you for this interesting review paper on smoke optical properties. We have incorporated it in the new version to discuss the values used in the ALADIN-Climate model.

195 Line 242: See comment on line 171

Please, see above concerning the use of a new simulation with different e-folding time.

200 Line 247: this ratio is also a bit high. Consider, OC makes up about 40-50% of mass, so a ratio of 2.3 makes over 100% of mass, and we know that Africa smoke is dominated by grass fires which have a high inorganic fraction.

205 ***We agree on the fact that there are strong uncertainties on the POM to OC ratio. In this work, we have finally retained the value of Formenti et al. (2003). However and due to this large uncertainty, we have also conducted additional sensitivity tests using two different values (2 and 3) of the POM to OC ratio. The results are presented in the Figure S1 (Appendix) showing an important sensitivity of ~0.2 on AOD over the box 5-15S/15-25E. This point is now more discussed in the new version.***

Line 284: I think the site is now Mongu Inn instead of Mongu

This is now changed.

210 Line 293: Which AERONET version was used? V3 came on line recently so it is not obvious.

We have used version2/level 2 AERONET retrievals. This point is now detailed in the new version.

Line 326: What was the altitude above clouds the reflectance was taken at?

215 ***The reflectance measurement was taken at 1430 m, just prior to the profile. In-situ cloud data shows cloud top heights at 600m. In that sense, the reflectance has been measured about ~800 m above cloud tops. This specific point is now mentioned (Part 3.2.3.2).***

Line 554; CALIOP is all CAPS

This is changed.

220

Line 627: How much do you think assumptions of hygroscopicity versus speciation plays into this? Granted, this is mostly an absence of BC in smoke, but you still may have a factor of 2 floating around given the high RH in the MBL.

225 ***We think the bias is mostly due to the aerosol speciation in this case. Hygroscopic properties that we used in the model is not able to explain such important differences in SSA. In addition, an external mixing hypothesis is used in the model, excluding the possible « lensing » effect (associated to increase of absorption).***

Line 635: can you elaborate here?

230 ***This point is now more detailed in the new version.***

Paragraph around Line 683: This paragraph is bordering on a non-sequitur. Wv is a great tracer, but is fundamentally different from RH. So careful how you talk about humidity and optical properties.

This is effectively right and we have now modified this paragraph.

235 Paragraph around 695: Can you compare model versus measured f(RH) directly here?

This point is a very interesting but, unfortunately, we could not conserve in the model both the dry and wet optical properties of smoke aerosols and we only calculate the wet properties for direct comparisons with in-situ/satellite observations.

240 Paragraph starting 760:

On PBL impact: Please be specific what you mean by PBL height, are you referring to the actual top of the PBL (that can be somewhat amorphous given the depth of the entrainment zone in cloud atmospheres, but comes out often as a hazy model metric) or are you referring specifically to the top of the mixed layer? If you are referring to a systematic change in the base of the inversion, please state that clearly throughout. Also, Just curious, any wind impacts? Mark Jacobson years ago was reporting big wind impacts in global GATOR simulations. See any evidence? Regardless positive or negative it is worth mentioning any notable wind impacts.

245 ***In this study, the PBL height corresponds to the top of the PBL. This is now detailed in the text. In parallel, we have also investigated the impact of BBA on the near-surface (10m) wind speed. The results are presented in the following figure. In our case, we obtain a general decrease (of about -0.5 m.s^{-1}) of the surface wind over most of the continent. Over the ocean, the impact of BBA is more complex with the presence of a regional contrast, characterized by an increase (decrease) of the surface wind around $0-10^{\circ}\text{W}/15-30^{\circ}\text{S}$ (latitudes higher than 15°S). This point is now mentioned in the part 5.2 of the new version.***

255

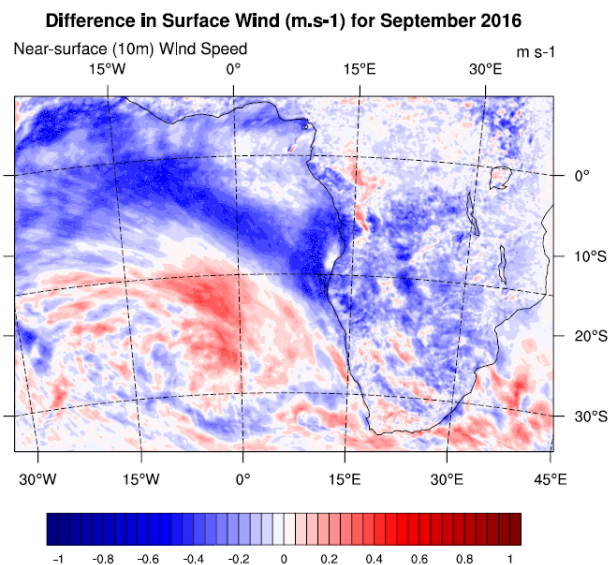


Figure indicating the changes in the surface wind speed due to BBA (averaged for September 2016).

280 Also, can you calculate a specific surface temperature change per unit optical depth? See this for comparison <https://www.atmos-chem-phys.net/16/6475/2016/>

285 ***This is an interesting remark and we have now calculated the changes of surface temperature per unit of AOD due to the presence of BBA. The results we obtained (averaged for all the period of simulation) is about -2.5° per unit AOD (at 550 nm). We observe that this value is consistent and higher to the one (-1.5°) published by Zhang et al. (2016) for a massive biomass burning event occurring over Central Canada***

290 *during June 2015. The difference could be due to the absorbing properties of BBA, which are more pronounced in the present study compared to Zhang et al. (2016) (SSA of 0.94). This could favor higher dimming effect and impact on the surface temperature over the Angola region. This interesting point is now mentioned in the part 5.2 and the reference of Zhang et al. (2016) is added.*

295

300

305

310

315

320

325

330

335

340

345

Referee 2

350 **Dear Editor,**

We first would like to thank the reviewer for all the remarks and suggestions that we used to improve the manuscript. We have tried to take into account most of the mentioned points.

355 Review of “Simulation of the transport, vertical distribution, optical properties and radiative impact of smoke aerosols with the ALADIN regional climate model during the ORACLES-2016 and LASIC experiments” by Mallet et al., submitted to Atmos. Chem. Phys.

360 In this study, the authors compare a simulation of stratocumulus clouds and biomass-burning aerosols over the southeastern Atlantic to aircraft and satellite retrievals of clouds and aerosol properties. They find that the simulation is satisfactory in the first order, although aerosol extinction and absorption and cloud fraction are underestimated, and cloud optical thickness is overestimated. A simulation nudged to reanalysis outperforms the free-running model because nudging improves simulated relative humidity, which in turns improves aerosol extinction through hygroscopicity.

365 The paper is interesting and well-written. Many aspects of modelled aerosols and clouds relevant to the direct radiative effects of biomass-burning aerosols are evaluated against multiple observational datasets. The discussion is convincing and supported by a large number of figures.

370 I have only one main comment: the authors should clearly set expectations in section 3, by which I mean to state clearly what the model should be capable of in terms of reproducing spatial and temporal variability, and what comparison the satellite products are able to usefully provide. The reason it matters is that the model seems to be using monthly-averaged emissions, which may not even be for the year 2016. So the model cannot be expected to reproduce daily distributions, even when nudged. In addition, temporal
375 sampling of satellite retrievals is limited, as stated by the authors, which means that model and observations should really be co-located temporally before being compared (Schutgens et al. doi:10.5194/acp-16-1065-2016 2016). This is not done here consistently, so there the comparisons can only be qualitative. In addition, I note that it is becoming more challenging to avoid circular reasoning, i.e. not comparing models using satellite-derived emissions to the same satellite products, and to reanalyses that assimilate some of those
380 same products. This is not a criticism of the paper, but it suggests that having multiple, independent observational datasets for the same variables is becoming increasingly important.

***This is effectively right, and represents an important limitation for the comparisons between models and satellite observations. As remarked by the reviewer and concerning the emissions, we have now clearly
385 stated in the new version (section 3.1) the methodology used in this study and what the model is able to reproduce. We especially point out the fact that comparisons are only « qualitative ». Indeed, the ALADIN-Climate simulation used « monthly-mean » biomass burning historical CMIP6 emissions, based on historical GFED emission. The reference which presents these CMIP6 emissions (van Marle, et al., 2017) is now provided in the new version. The main point of the methodology ; namely the use of the Global Fire Emissions Database version 4 (GFED4s) for the 1997–2015 period, is now indicated in the text.***

***In this work, the ALADIN-Climate simulation used the « monthly-mean » emission for one of the closest
395 year of the historical CMIP6 emissions; namely the year 2014, as 2016 is not available. This methodology implies « realistic » emissions in terms of magnitude but does not represent daily variations. This important point is now detailed and discussed in the different parts (sections 3.1 and 4.2.1 notably) to underline our methodology and clearly point that this does not allow the model to reproduce precisely daily aerosol distributions over SAO.***

***It should be noted here that our main motivation was to use the ALADIN-Climate model in its « climate»
400 configuration to study its ability at reproducing the main cloud and aerosol optical properties over the SAO. This represents a crucial and necessary step before using such regional climate model in an exactly similar configuration at climatic scales to address the radiative and climate impact of BBA over Southern***

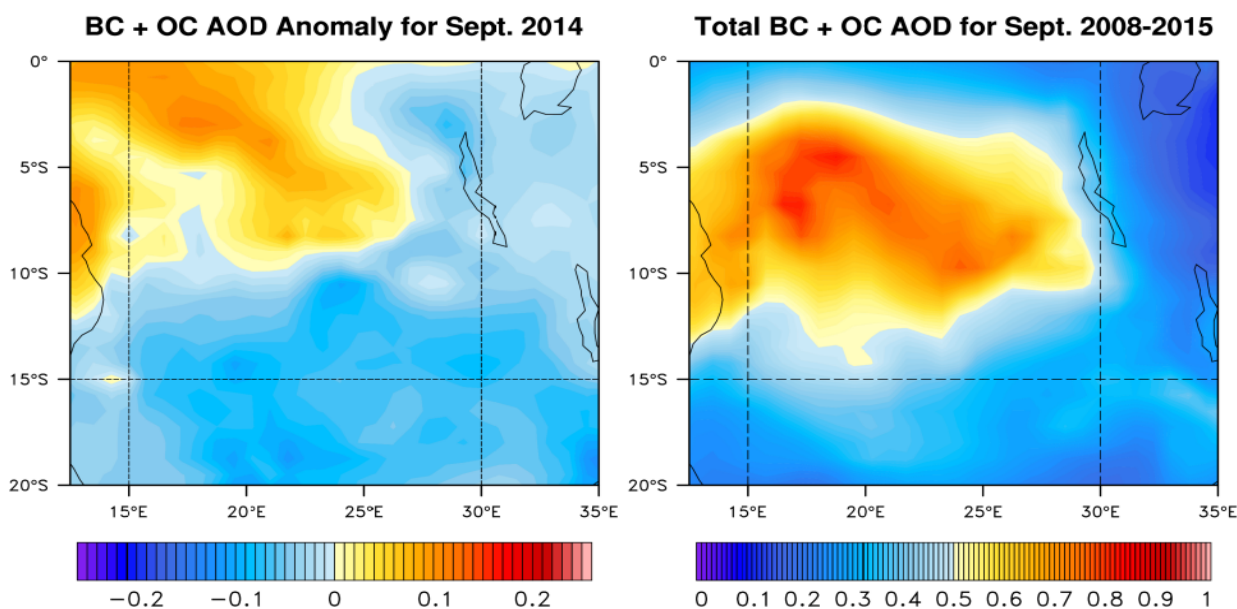
Africa, which clearly represents the main vocation of such a modeling tool, compared to meso-scale fine resolution models (such as WRF-C). We remind this important aspect in the new version (section 3.1).

405

In parallel, we have checked that the BC+OC AOD for September 2014 was found to be consistent, in terms of AOD, to CAMS climatology for the 2008-2015 period. The 2014 september anomaly (see the following figure now provided in Appendix) indicates small differences $\sim 0.05-0.10$ over the BBA sources for September 2014 compared to the climatology. Additionally, Sayer et al. (2019) found similar above-cloud and total-column AOD over the southern Atlantic Ocean in 2014 and 2016. This would suggest that the effect of potential differences between 2014 and 2016 for BC-OC emissions over the biomass burning region is likely to be small. These points are now underlined in the part 3.1 of the new version. The following reference has been added.

410

415 Sayer et al., Two decades observing smoke above clouds in the south-eastern Atlantic Ocean : Deep Blue algorithm updates and validation with ORACLES field campaign data, Atmos. Meas. Tech. Discussion, in review, 2019.



420

New Figure S1. September 2014 BC-OC AOD anomaly (left) compared to the 2008-2015 period (September month only) and the total mean BC+OC AOD for the 2008-2015 period (right) from CAMS reanalyses. This figure is now provided in the new version of the Appendix.

425

Concerning the comparisons with satellite data, we have also mentioned in the new version the uncertainties/limitations related to the use of monthly-mean emissions to force the model. In addition, all the comparisons between the ALADIN-Climate model and satellite retrievals have been performed by using only ALADIN-Climate outputs at the different satellites (OMI, MODIS) over-passing (i.e., between 10:30 & 13:00 UTC). This is now indicated in the new version and clearly stated for the figures 3 and 4. In parallel, the figure 6 has been modified using MODIS and OMI equator crossing times (10:30 and 13:30 UTC) for the ALADIN-Climate outputs. This leads to moderate changes in the simulated ACAOD (small decrease) over the continent.

430

Addressing my main comment, and the other comments below, should represent minor revisions.

Other comments:

435

Line 63: It would be good to define DRF here: with respect to no-aerosols. Note that the IPCC calls that direct radiative effect (DRE). Forcing is when defined with respect to pre-industrial aerosols.

This is right and now mentioned in the new version.

440 Line 65: the “well-known” cooling effect is only true on a global average, so there is no contradiction really. I suggest rephrasing to contrast the top-of-atmosphere radiative effect of scattering and absorbing aerosols.
This is right and changed in the text.

Line 78: Which domain?
445 ***The domain (4–18°S, 5°W–14°E) is now defined.***

Lines 111–112: What are the roles of AEROCLO and CLARIFY in this paper ?
This was only a point of the general context, indicating the different programs conducted over this region with co-incident experimental campaigns. We think that this is of interest to mention in the introduction but we can remove it if necessary. We have clearly stated that only the data from LASIC and ORACLES programs have been used in this work.
450

Line 142: It would make more sense to start the chain of processes with surface emissions.
This is now modified in the new version.
455

Line 160: “also represented” – I suppose that semi-direct effects do not have a dedicated representation in ALADIN. They implicitly derive from direct effects.
This is right and we have now replaced « also represented » by « is derived from the direct effect ».

460 Lines 164–165: Strictly speaking, smoke is often anthropogenic – it is just that emission people cannot tell the two components apart so call the dataset “biomass-burning”.
This is noted. We prefer to keep the term « biomass-burning » in the text to avoid confusions with BC and OC emissions from anthropogenic activity.

465 Line 169: Is the fresh mode hygroscopic?
Yes. This specific mode has lesser hygroscopic properties than aged smoke, as reported in the relation 1 and Table 2. This point is now precised.

Line 172: “more aged” is unclear. Once in the aged mode, aerosols cannot aged further in the model. Or are you saying that an e-folding time of 3 or 6 hours won’t make much difference for SAO properties ?
470 ***We rewrote this sentence : « The smoke over the SAO is expected to have aged by 5-7 days...».***

Line 183: Is that the mean over the year or over the biomass-burning season? The latter would make more sense.
475 ***This is the mean value over the year, and further developments are needed to better take into account the seasonal variations of smoke optical properties (especially from grass to forest burning). This clearly represents one limitation and following this remark (as also noted by the reviewer 1), we have added a new simulation, SMK_SSA using SSA of 0.92 to test the sensitivity of BBA absorbing properties on SW heating, direct forcing, surface temperature as well as the PBL development. We have now indicated the additional results in the new Figure 13 and Figure S7 (provided in Appendix). In parallel, the results are also summarized in a new Table (Table 3).***
480

In terms of SW radiative heating and direct radiative forcing, this additional simulation indicates :

485 - a significant decrease of the SW radiative heating induced by smoke aerosols. For example and over the Box_S (defined over the sources of biomass burning), SW heating at 3km is passing from +1.15°K by day to + 0.58°K by day. This result moderates the SW heating induced by smoke at the end of the biomass burning season. This specific point is now included in the article (paragraph 4.2.4.3) and in the new Table 3,
490

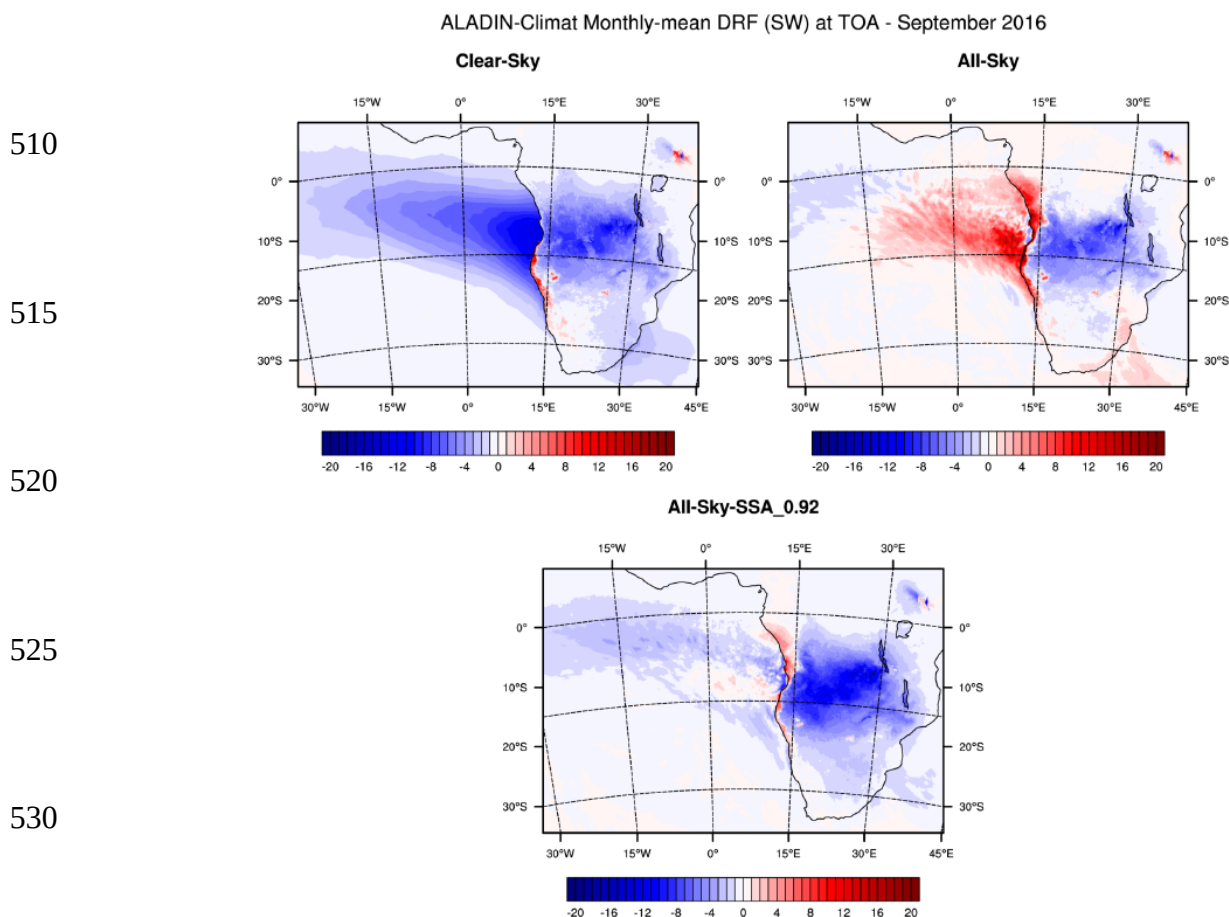
- a significant change in the monthly-mean (September 2016) DRF at TOA, passing from a positive (+4.2 W.m⁻²) to negative (-0.54 W.m⁻²) direct forcing (see new Figure 13 and Table 3) over the Box_O (ocean). This means that the positive direct forcing at TOA could be lesser in intensity at the end of the BBA season (late october). This important point is now mentioned in the part 5.1 and the results of the new

495 *ALADIN-Climate (SMK_SSA) simulation including more scattering BBA (SSA of 0.92 at 550 nm) are included in the Table 3,*

500 *- a more intense negative DRF at TOA over smoke sources due to more scattering BBA. Over the box_S, the monthly-mean value (Table 3) is increasing from -3.9 W.m^{-2} (SMK) to -7.3 W.m^{-2} (SMK_SSA). This specific point is added in the disussions and in the Table 3,*

- a less pronounced positive DRF at TOA along the Southern African coast and Gabon due to more scattering BBA (now indicated in the paragraph 5.1),

505



535

New figure 13 including (bottom) the monthly-mean DRF exerted at TOA for more scattering smoke aerosols (SMK_SSA ALADIN simulation).

540 *Concerning the impact of BBA on other variables (SW radiations at the surface, surface temperature, sensible heat fluxes and PBL height), we did exactly the same figure as Figure 14 but for the new simulation (SSA_SMK). This new figure has been added in Supplement material (S8) and the main results are discussed in the Part 5.2. We have notably added these clarification's :*

545 *« Finally, the comparisons with the SMK_SSA simulations (not shown, Figure S8) indicate a decrease of the surface radiative forcing both over continent and ocean. As reported in Table 3, the monthly-mean DRF at BOA is about -39 W.m^{-2} and -25 W.m^{-2} over Box_S (biomasse burning sources) for the SMK and SMK_SSA simulations, respectively. The same result is obtained over SAO. This is due to the decrease of SW radiations absorbed by smoke in the SMK_SSA simulation, increasing the SW radiations reaching the surface. This could be also due, to a lesser extent, to some changes in aerosol loading due to*

550 *modifications in the dynamics and precipitation between the two simulations. This induces a less pronounced impact of BBA on the surface temperature and sensible heat fluxes in the SMK_SSA run. The increase of SW surface radiations, associated to low absorption by BBA in SMK_SSA, decrease the impact of smoke on the PBL development (Figure S8). As mentioned previously, these results suggest that the impact of BBA on the surface fluxes and dynamics are certainly slightly lower at the end of the biomass burning season. »*

Line 227: “forced-mode configuration” is ambiguous – does that mean fixed SSTs ?
This is effectively the case. This point is now clearly mentioned.

560 Line 229: Need more information about those CMIP6 emissions, including a reference. This is a crucial aspect of the model, which will influence its capabilities and the interpretation of the comparison to observations. Is the dataset GFED- or GFAS- (i.e. satellite-)based? Are emissions really for the given year or just interpolations between key years, liked they did in CMIP5?

565 *As mentioned above, the biomass-burning emission used in the model are monthly-mean values based on GFED inventory database. The reference (van Marle, et al., 2017) describing the methodology to build CMIP6 emission are now indicated in the new version. CMIP6 emissions are developed with realistic-timing emission for the 1997-2015 period but not for 2016. This point is now clearly mentioned in the new version associated with the related limitations.*

570 *van Marle, M. J. E., Kloster, S., Magi, B. I., Marlon, J. R., Daniau, A.-L., Field, R. D., Arneeth, A., Forrest, M., Hantson, S., Kehrwald, N. M., Knorr, W., Lasslop, G., Li, F., Mangeon, S., Yue, C., Kaiser, J. W., and van der Werf, G. R.: Historic global biomass burning emissions for CMIP6 (BB4CMIP) based on merging satellite observations with proxies and fire models (1750–2015), *Geosci. Model Dev.*, 10, 3329-3357, <https://doi.org/10.5194/gmd-10-3329-2017>, 2017.*

575 Line 234: The boundary layer is probably deeper than just the first model level.
This is right and our sentence is confusing. We would like to indicate near the main biomass burning sources and not the surface layer. This sentence is now rephrased in that sense.

580 Line 235: The Dentener recommendations are more complex that just injecting into the first model level. See their Table 2.
This is right. This point is now modified and we have now removed the following sentence : « smoke emissions force the model at the first model level following the recommendations from the first phase of AEROCOM ».

585 Line 244: Is the ratio applied to the emissions or when mass is transferred from the fresh to the aged mode ?
This is done when the mass is transferred from the fresh to aged mode in the model. This point is now stated.

590 Line 253: Worth noting that 0.15 represents about 20% of BBA AOD, so not a small change.
This is right and we have now rephrased the sentence to indicate that changes could be important for smoke AOD.

595 Lines 298–302: Why is that a good thing for aerosol retrievals? Better correction of the Rayleigh contribution?
To clarify how this helps aerosol retrievals, we have edited the sentence like this: “...but not aerosol scattering. This channel therefore provides a direct observation of the attenuation of the signal and allows for the direct calculation of aerosol extinction without external constraints or assumptions on the aerosol optical depth or lidar ratio.”

600 Line 364: “ice clouds are not processed” is unclear. Does that mean that scenes containing ice clouds are discarded completely?

This is effectively the case and the scenes containing ice clouds are discarded completely. It should be noted that the different boxes used to evaluate the model are characterized by negligible high cloud fraction.

605

Line 386: Does that retrieval suffers from the issues raised by Haywood et al. doi:10.1256/qj.03.100 (2004)? If so, that is a problem for the present study.

610

This is a good remark and the possible effect of the presence of BBA on the stratocumulus properties retrievals has been studied and quantified recently by Seethala et al. (2018). This study indicates that, in the aerosol-affected months of July–August–September, SEVIRI LWP (based on the 1.6 μ m Cloud Effective Radius) is biased by ~16%. This point is now clearly indicated in the new version and the following reference has been added.

615

Seethala, C., Meirink, J. F., Horváth, Á., Bennartz, R., and Roebeling, R.: Evaluating the diurnal cycle of South Atlantic stratocumulus clouds as observed by MSG SEVIRI, Atmos. Chem. Phys., 18, 13283-13304, <https://doi.org/10.5194/acp-18-13283-2018>, 2018.

Lines 395–396: Suggests shortening the title to “Reanalyses of atmospheric composition”.

620

This is changed.

Line 424: But at this stage of the analysis, it is not yet known that clouds are too bright – it will be shown in the following section.

This is effectively right and we have now changed the sentence in the part 4.1.1.

625

Line 431: What kind of parameterizations are they?

The two parameterizations concern the calculation of the liquid cloud optical depth (COD) using LWP and Cloud effective radius but with different coefficients depending of the wavelengths. This point is now detailed.

630

Lines 441–442: It would be worth noting that indirect effects are relevant to DRF, because DRF depends on the albedo of the underlying stratocumulus.

This is right and now added in the new version.

635

Line 448: Note that the CAMS Reanalysis, successor to MACC, covers 2016, so could be added to the comparison. See <https://apps.ecmwf.int/data-catalogues/cams-reanalysis/?class=mc&expver=eac4>

This is an interesting point and the total AOD from CAMS reanalysis has been now added in the new Figure 3 and discussed in the text.

640

Lines 455, 477, and 482: Those large differences are surprising because MERRA is supposed to be assimilating MODIS! Perhaps a different collection? The fact that MERRA assimilates MODIS should explain the good temporal correlation, though.

To our knowledge, MERRA does not assimilate these MODIS products; it does a neural network-based retrieval on the MODIS radiances and assimilates the results of that instead. This leads to a better (compared to ALADIN-Climat) temporal correlation, which is now mentioned in the new version.

645

Lines 458–472: I agree that land-ocean contrast in satellite products are worth investigating further. At first, I though that marine aerosols could possibly explain why there is more AOD over ocean than over land. But if we assume that the contrast observed on Figure 3 south of the BBA plume, say 20S, is only due to seasalt, we only get about +0.1 contrast. Reporting that to within the plume leaves about 0.1-0.2 of contrast unexplained.

650

This is an interesting remark, which is now added in the text to explain part of the AOD contrast between land and ocean.

655

Line 462: MODIS products include uncertainties so it is a good place to use them. Perhaps show an uncertainty range on Figure 4?

This is now done using uncertainties provided by Sayer et al. (2016) and Gupta et al. (2018), for Deep Blue ACAOD and Dark Target AOD aerosol products, respectively.

660 Line 472: “more robust” – in terms of sampling yes, but the AOD retrievals are also more uncertain over land than over ocean because the surface albedo is larger.
This is right and the term « robust » is not appropriated and now removed.

665 Line 509: How is ACAOD calculated in the model? It is not always easy to determine where the cloud top is.
It is calculated as the integration from the model top to the cloud top. This point is now detailed.

670 Lines 523–524: What did Shinozuka et al. Find?
Shinozuka et al. indicate similar results than presented in this work, especially an underestimate of the simulated ACAOD with the ALADIN-Climate model for different boxes defined over the SOA region. This specific point is now detailed in the new version.

Lines 531–539: That analysis supports the idea that injection heights are not that important. Aerosols are lofted by convection anyway.
This is right and this point is now added.

675 Line 552: Is the decrease in extinction driven by a decrease in mass?
The decrease in extinction is effectively mostly driven by a decrease in the BBA concentration. This is precised in the text.

680 Line 562: The statement on advection contradicts line 141. I fail to see why the model could not represent those BBA incursions into the BL – it might be that the model of Gordon et al. is wrong!
The term « advection » is not appropriated and we have now modified it. In addition, we have moderated this point indicating that the results obtained with ALADIN are different from those obtained by Gordon et al. (2018).

685 Line 587–589: So the RH biases go in the right direction to (partly) explain the extinction biases.
This is right and added in the new version.

690 Line 615: The agreement is good but observational uncertainties are large.
This is true and the uncertainties related to SSA AERONET retrievals are now indicated in the part 4.2.4.1.

695 Lines 624–632: That paragraph is confusing. Is the comparison fair? Is the model simulating BBA on the days of the comparison? Can we be sure that LASIC is observing transported BBA and not local sources?
The comparison has been done effectively for each days (daily mean) with the SSA observed at the surface at the ascension island ARM site. An important point is that the LASIC site is located on the remote windward side of the island and is not affected by local sources, of which there are few to begin with (no trash burning on the island). This is precised in the article.

700 Line 633: “reflect” – the observations are insufficient to link that absorption to ageing during transport. I am not convinced the model is wrong here.
This point is effectively not enough detailed. One indication that the aerosol sampled at the LASIC is aged is through the parameters f44 and f60, the fraction of the organic aerosol mass spectrum signal at m/z 44 and 60 respectively, in the data from the Aerosol Chemical Species Monitor (Alison Aiken, personal communication). The LASIC f44 and f60 values of approximately 0.2 and 0.002 respectively are characteristic of highly aged aerosols (Cubison et al., 2011). All these points are now included.

710 ***Cubison, M. J., Ortega, A. M., Hayes, P. L., Farmer, D. K., Day, D., Lechner, M. J., Brune, W. H., Apel, E., Diskin, G. S., Fisher, J. A., Fuelberg, H. E., Hecobian, A., Knapp, D. J., Mikoviny, T., Riemer, D., Sachse, G. W., Sessions, W., Weber, R. J., Weinheimer, A. J., Wisthaler, A., and Jimenez, J. L.: Effects of aging on organic aerosol from open biomass burning smoke in aircraft and laboratory studies, Atmos. Chem. Phys., 11, 12049-12064, <https://doi.org/10.5194/acp-11-12049-2011>, 2011.***

- Line 650: Are all those studies based on modelling?
Yes and this is now stated in the text.
- 715 Line 674: Section 4.3 is interesting. Essentially aerosol DRF errors in the SAO are driven by non-aerosol aspects. It is however unclear if the increased water vapour is due to the fires or because of transport in convective air masses. I suppose it is the latter, since the model does not emit water vapour with fires, nor does it account for additional buoyancy from the fires. Although lines 722–723 are ambiguous about what the model really does.
- 720 ***This is an open interesting question which is not resolved at this time to our knowledge. We agree with the reviewer that the presence of water vapor could be due at the first level to convective air masses as indicated by Adeyemi et al. (2015). In parallel, it is known that fires release important concentration of Wv but such processes are totally absent in the model at this time. This would represent interesting developments. This point has been detailed in the new version (3.1).***
- 725 Line 554: “we suspect”. We were promised a bit more. Can we have an integrated assessment of what the different model biases in CF, COD, ACAOD, and SSA mean for DRF?
This is an interesting remark, which represents an important work, notably by performing new sensitivity tests, based on additional simulations including variations of each variables (CF, COD, ACAOD and SSA) independantly. These new simulations/tests are unfortunately outside the scope of the article.
- 730 Table 2: It would be useful to add a column listing the periods covered by each product.
This is now inserted in the new Table 2.
- 735 Technical comments:
- Line 105: Consist to -> is to
This is modified.
- 740 Line 187: g has not yet been defined, unless I missed it.
This is effectively right and corrected in the new version.
- Line 221: The definition of the domain encompasses the main biomass-burning sources of that region, and also the transport to the Atlantic ocean.
- 745 ***The ALADIN-Climate domain used to realize the simulation (Latitude : -37.1°S to 09.4°N ; Longitude :-33.4°W to 45.4°E) is now clearly indicated in the Part 3.1.***
- Line 224: Suggest moving the Mlawer reference to line 155 for consistency with FMR.
This is changed.
- 750 Line 234: Not sure “accordingly” is the right word here.
This is right and « accordingly » has been changed by : « In the simulations, ... »
- Line 241: produce -> produced
- 755 ***Now changed.***
- Line 357: CER has not yet been defined.
This is modified in the new version.
- 760 Figure 7: Could the orography be put in a colour that is not in the colour scale used for aerosol extinction? Grey perhaps?
This is changed in the new Figure 7.

765 **Simulation of the transport, vertical distribution, optical properties and
radiative impact of smoke aerosols with the ALADIN regional climate
model during the ORACLES-2016 and LASIC experiments.**

Marc Mallet¹, Pierre Nabat¹, Paquita Zuidema², Jens Redemann³, Andrew Mark Sayer^{4,5}, Martin
770 Stengel⁶, Sebastian Schmidt⁷, Sabrina Cochrane⁷, Sharon Burton⁸, Richard Ferrare⁸, Kerry Meyer⁵,
Pablo Saide⁹, Hiren Jethva^{4,5}, Omar Torres⁵, Robert Wood¹⁰, David Saint Martin¹, Romain Roehrig¹,
Christina Hsu⁵ and Paola Formenti¹¹

Affiliation

775 ¹ Centre National de Recherches Météorologiques, UMR3589, Météo-France-CNRS, Toulouse, France

² Rosenstiel School of Marine and Atmospheric Sciences, University of Miami, Miami, FL, USA

³ University of Oklahoma, USA

⁴ Universities Space Research Association, Columbia, MD, USA

⁵ NASA Goddard Space Flight Center, Greenbelt, MD, USA

780 ⁶ Deutscher Wetterdienst (DWD), Offenbach, Germany

⁷ University of Colorado, Boulder, USA

⁸ NASA Langley Research Center, Hampton, Virginia, USA

⁹ University of California, Los Angeles (UCLA), USA

¹⁰ University of Washington, Seattle, USA

785 ¹¹ Laboratoire Interuniversitaire des Systèmes Atmosphériques, UMR CNRS 7583, Université Paris Est
Créteil et Université Paris Diderot, Institut Pierre Simon Laplace, France

Correspondence to: M. Mallet (marc.mallet@meteo.fr)

790

795

Abstract

Estimates of the direct radiative forcing (DRF) from absorbing smoke aerosols over the Southeast Atlantic Ocean (SAO) require simulation of the microphysical and optical properties of stratocumulus clouds as well as of the altitude and shortwave (SW) optical properties of biomass burning aerosols (BBA). In this study, we take advantage of the large number of observations acquired during the ORACLES-2016 and LASIC projects during September 2016 and compare them with datasets from the ALADIN-Climate regional model. The model provides a good representation of the liquid water path but the low cloud fraction is underestimated compared to satellite data. The modeled total column smoke aerosol optical depth (AOD) and Above Cloud AOD are consistent (~ 0.7 over continental sources and ~ 0.3 over SAO at 550 nm) with MERRA2, OMI or MODIS data. The simulations indicate smoke transport over SAO occurs mainly between 2 and 4 km, consistent with surface and aircraft lidar observations. The BBA single scattering albedo is slightly overestimated compared to AERONET, and more significantly when compared to Ascension Island surface observations. The difference could be due to the absence of internal mixing treatment in the ALADIN-Climate model. The SSA overestimate leads to underestimate the simulated SW radiative heating compared to ORACLES data. ~~For September 2016,~~ ALADIN-Climate simulates a positive (monthly mean) SW DRF of about $+6 \text{ W}\cdot\text{m}^{-2}$ over SAO (20°S – 10°N and 10°W – 20°E) at the top of the atmosphere and in all-sky conditions. Over the continent, the presence of BBA is shown to significantly decrease the net surface SW flux, through direct and semi-direct effects, which is compensated by a decrease (monthly mean) in sensible heat fluxes ($-25 \text{ W}\cdot\text{m}^{-2}$) and surface land temperature ($-1.5 \text{ }^{\circ}\text{C}$) over Angola, Zambia and Congo notably. The surface cooling and the lower tropospheric heating decreases the continental planetary boundary layer height by about $\sim 200 \text{ m}$.

1. Introduction

Southern Africa is one of the main sources of biomass burning aerosols (BBA) at the global scale. When the intense smoke plumes are transported over the Southeast Atlantic Ocean (SAO), they are able to produce a significant positive (**warming**) direct radiative forcing (DRF; **with respect to no-aerosols**) at the top of the atmosphere (TOA) in the SW spectral range and in all-sky conditions (De Graaf et al., 2012, 2014, Feng and Christopher, 2015, Zuidema et al., 2016). Over this specific region, the sign of the DRF is found to be opposite to the ~~«well-known»~~ cooling effect generally exerted by ~~natural and anthropogenic~~ scattering aerosols at TOA. Based on the combination of satellite observations from A-Train data sets (MODIS, CERES and OMI), Feng and Christopher (2015) indicate a regional-averaged instantaneous (i.e., time of observations) DRF of about $+37$

W.m⁻² (regional mean; 20°S–10°N and 10°W–20°E) for August 2006, with the highest magnitude of the forcing reaching +138 W.m⁻² at TOA. Significant positive values are also underlined by De Graaf et al. (2012, 2014), who estimate an averaged DRF (August 2006) of about +23 W.m⁻² near the Southern African coast. In parallel, Meyer et al. (2013) report an instantaneous (near local noon for Aqua overpass) regional mean above-cloud radiative forcing efficiency from 50 W.m⁻²AOD⁻¹ to 65 W.m⁻²AOD⁻¹ by using their bias-adjusted MODIS cloud retrievals. By using SCIAMACHY observations and radiative transfer model calculations, De Graaf et al. (2014) further estimate a SW DRF of about ~+ 30/35 W.m⁻² over the same domain (4–18°S, 5°W–14°E) in August and September (2006-2009).

This positive sign (warming) of the DRF is mainly due to the presence of highly reflective stratocumulus clouds (Sc) over the SAO. Although such a positive DRF is occasionally observed over other regions, such as the northeast Pacific during extreme summertime biomass burning events in continental North America (Mallet et al., 2017), the SAO clearly represents the main region at the global scale where such positive forcings can be observed every years at a seasonal-time scale. Indeed, this significant radiative forcing is due to the persistent biomass burning emissions over Central Africa during the July-August-September-October (JASO) period. Smoke emissions over the central Africa are also related to a significant inter-annual variability, associated with an important increase over the 1979-2015 period (Hodnebrog et al., 2016).

All studies clearly underline the importance of both the aerosol radiative properties of smoke plumes (e.g., Aerosol Optical Depth, AOD, single scattering albedo, SSA), their vertical structures (notably, the localization of smoke vs. Sc; Johnson et al., 2004) as well as the underlying cloud properties (e.g., cloud optical depth (COD), liquid water path (LWP)) on the produced positive SW DRF at TOA. As an example, Feng and Christopher (2015) report a critical COD of ~12-20 capable of changing the sign of the DRF from negative to positive (at TOA) for BBA characterized by SSA ~0.91 and AOD ~1.0 (at 550 nm). In the case of more absorbing smoke (SSA ~0.85), the ranges for critical COD are strongly reduced and reach ~2-4. Chand et al. (2009) also underline the importance of cloud coverage on the DRF exerted at TOA by smoke over SAO. In addition, Sakaeda et al. (2011) provided model estimates of regional radiative forcing from direct and semi-direct effects, with important implications on cloud properties (cloud fraction notably). These complex processes, involving both microphysical and optical properties of BBA and Sc explain, at least partially, the large difficulty of recent global climate models (GCM) in reproducing the DRF of smoke over this specific region (Stier et al., 2013).

In that context, it appears crucial to evaluate carefully and constrain both smoke aerosols and Sc properties in GCM or in their regional configurations (regional climate models, RCM) before

running them over a long-time period, for radiative budget and climatic considerations. The main objectives of this study ~~is consist~~ to investigate the transport of BBA over SOA, the vertical layering as well as optical properties using the ALADIN-Climate model. In addition, the induced SW DRF at TOA and the possible impact of BBA on the regional (continental) climate are also
870 analysed. This work has been conducted in the context of several international field campaigns over the SAO region, including the ObseRvations of Aerosols above Clouds and their intEractionS (ORACLES) (Zuidema et al., 2016), the Layered Atlantic Smoke Interactions with Clouds (LASIC, Zuidema et al., 2018), the AErosol RAdiation and CLOuds in Southern Africa (AEROCLO-sA) and the Cloud-Aerosol-Radiation Interactions and Forcing : Year 2017 (CLARIFY) projects. More
875 specifically, this study takes advantage of the large number of in situ observations acquired from aircraft and surface measurements during September 2016 for the ORACLES-1 and LASIC projects. This unique dataset is combined to satellite aerosol and cloud retrievals (MODIS, OMI and SEVIRI) and re-analysis (MERRA2, CAMS and MACC) data.

We focus our analyses on specific properties which are important to study the radiative effect of
880 BBA over SAO. For Sc clouds, these are low cloud fraction (LCF), liquid water path (LWP) and COD. For BBA, special attention is paid to AOD, Above Cloud AOD (ACAOD), extinction vertical profiles, SSA, and SW radiative heating due to smoke. The DRF at the surface and TOA are estimated and analysed in addition to climatic implications, especially those exerted by BBA over the Central Africa continent. The regional modeling model used in this work is the ALADIN-
885 Climate model (Nabat et al., 2015a, 2015b; Daniel et al., 2018), which has been modified in a recent configuration to better represent smoke aerosols and notably their SW optical properties.

This article is organized as follows. First, details on these recent developments are provided in section 2 as well as the design of the ALADIN-Climate simulations. Section 3 reports the complete dataset (satellites, reanalysis, in situ surface and aircraft observations). The analyses of the
890 comparisons between simulated and observed Sc and aerosol properties are presented in section 4. Based on the comparisons, we analyse more specifically the concentration of smoke aerosols over biomass burning sources and during the transport, the altitude of BBA, as well as absorbing properties and induced SW heating rate due to smoke. In addition, the impact of the elevated relative humidity within smoke plumes on optical properties is also investigated in section 4. Finally,
895 section 5 focuses on the analyses of the SW DRF exerted by smoke aerosols at TOA during September 2016, as well as their impact on the continental climate in terms of the surface energy budget (temperature, sensible heat fluxes) and lower troposphere dynamics (planetary boundary layer (PBL), notably).

2. The regional ALADIN-Climate model

900 **2.1. Aerosol Scheme**

The recent aerosol scheme (TACTIC, Tropospheric Aerosols for Climate in CNRM-CM) included in the ALADIN-Climate model accounts for sulfate, organic (OC) and black (BC) carbon, dust and primary sea-salt particles (Nabat et al., 2015b; Michou et al., 2015). **The biomass-burning emissions from the CMIP6 inventory have been used for BC, OC and sulfur gaseous SO₂. In ALADIN-Climate, mineral dust and sea-salt emissions are interactively connected with surface meteorological fields and soil properties (Nabat et al., 2015a). The emission of mineral dust is taken into account following the Marticorena and Bergametti (1995) parameterization and the current formulation for primary sea-spray is based on Schulz et al. (2004).** This model includes advection by atmospheric winds, diffusion by turbulence, surface emissions as well as dry and wet (in-cloud and below cloud) removal processes.

For the primary BC and OC species and secondary sulfates, a bulk approach is applied whereby a fixed aerosol size distribution is assumed for calculating aerosol properties, while for mineral dust and sea salt particles, a more explicit size representation is used based on 3 bins for dust and sea-salt. The TACTIC scheme assumes an external mixture of the different aerosol species. For specific situations, this could potentially represent a limitation, especially with regard to possible BC mixing (internal/external) state, which can significantly affect SW absorption (Fierce et al., 2016) by aerosols. Knowing that, specific attention is being paid in this study to the simulated absorbing properties (SSA) of BBA, as well as the associated SW heating rate.

The radiative properties (mass extinction efficiency (MEE), SSA, and asymmetry parameter (ASY)) of each aerosol species are calculated for the different spectral bands of the Fouquart and Morcrette radiation scheme (FMR, Morcrette, 1989) and the rapid radiative transfer model (RRTM, **Mlawer et al., 1997**), for the SW and Longwave (LW) radiations, respectively. Aerosol DRF at the surface and at TOA (in SW and LW spectral range and for both clear-sky and all-sky conditions) is diagnosed using a double call (with and without aerosols) to the radiation schemes during the model integration. In addition, the semi-direct radiative forcing, which represents the modifications of the cloud properties and atmospheric dynamics due to absorption of SW radiations by smoke, **is derived from the direct effect**. In its current version, BBA are represented by two different tracers (primary BC and OC) with fixed microphysical and radiative properties without any consideration of possible differences between fossil fuel and biomass-burning emissions. This hypothesis implies that the radiative, hygroscopic properties and e-folding time (aging) of carbonaceous species are similar for both anthropogenic and smoke emissions.

2.2 Smoke Radiative properties

Two tracers have been recently implemented in ALADIN-Climate describing, respectively, the mass concentration of fresh (less hygroscopic) and aged (more hygroscopic) smoke aerosols, following the methodology presented in Bellouin et al. (2011). This allows to distinguish aerosols from biomass burning and anthropogenic emissions and to monitor specific properties, such as e-folding time, hygroscopic and optical properties. In the ALADIN-Climate model, aging from the fresh mode to hygroscopic aged is quantified using an e-folding time of 6 hours according to Abel et al. (2003). This value is two times higher than the one (~3 h) recently proposed by Vakkari et al. (2018) for southern African savannah. The smoke over the SAO is expected to have aged by ~~will be more aged, on the order of~~ 5-7 days (Adebiyi and Zuidema, 2017; Diamond et al., 2018). While studies of the BBA chemical composition and attribution for the smoke's optical and hygroscopic properties are still ongoing, preliminary results indicate further smoke aging increases its ability to function both as a cloud condensation nucleus and to absorb shortwave radiation (Zuidema et al., 2018).

For each tracer, dry-state aerosol size distributions are assumed based on lognormal function (Table 1) similar to those implemented in the Hadley Centre global climate model, HadGEM2-ES (Bellouin et al., 2011). The smoke dry-state refractive indices used to calculate radiative properties are also reported in the Table 1 (at 550 nm). The values of the real and imaginary refractive indices have been updated using the AERONET observations obtained by Eck et al. (2013) in Zambia (Mongu station). Although they indicate a pronounced seasonal cycle in the real and imaginary parts of the refractive index from AERONET data, we have used a mean value of 0.03 (at 550 nm) for the imaginary component in our Mie calculations (Table 1). This represents an important limitation and the seasonal cycle of smoke absorbing properties (average SSA at 440 nm from 0.83 in early July to 0.92 in mid-October, as noted by Eck et al., 2013) is not well represented in ALADIN-Climate. Due to period investigated in this study (August 2016), the implications are expected to be moderate as smoke are highly absorbing for this month over the continent and SAO (Eck et al., 2013, Zuidema et al., 2018). However, this would be a more severe limitation for simulations encompassing the full biomass burning season.

SW radiative properties have been calculated for the specific wavelength bands of the FMR radiation scheme. The values in the SW spectral ranges are reported in the Table 1. At 550 nm and in dry state, the calculated radiative properties are 4.05 m².g⁻¹, 0.84 and 0.51 for the MEE, SSA, and ASY g for the « fresh » smoke tracer (Table 1). The values for « aged » smoke are, respectively, 5.05 m².g⁻¹, 0.90 and 0.58 (Table 1). The MEE used in the model for « aged » smoke is found to consistent with those reported by Reid et al. (2005). As BBA are known to be hydrophilic (Rissler

et al., 2006), the dependence of the radiative properties to relative humidity (RH) has been included for both tracers. This dependence is formulated as described by Solmon et al. (2006) :

$$MEE_{\text{wet}} = MEE_{\text{dry}}(1-\text{RH})^{-\alpha} \quad (1)$$

where MEE_{wet} and MEE_{dry} are for wet and dry conditions. We have selected a value of 0.26 and 0.15 for the parameter α in order to reproduce the changes of MEE with RH for aged and fresh smoke, respectively. At very high humidity ($\text{RH} > 99\%$) maximum thresholds of 8.5 and 16.9 $\text{m}^2 \cdot \text{g}^{-1}$ are considered for fresh and aged smoke, in order to avoid unrealistic values of MEE. In a similar way, we have also implemented a dependence of smoke SSA on RH using the same relationship as (1) (Mallet et al., 2017). The values of α have been fixed to 0.015 (0.02) for aged (fresh) smoke to represent the variations of SSA with RH, as reported in Bellouin et al. (2011).

2.3 Aerosols and Cloud interactions

“Aerosol-cloud” interactions were represented using a simple parametrization, similar to most GCMs, thereby maintaining the low numerical costs necessary for climate and ensemble simulations. The activation of hydrophilic particles to cloud droplets is not explicitly resolved in ALADIN-Climate and the first indirect radiative effect is implemented for hydrophilic sulfates, organic carbonaceous and sea-spray aerosols. This first indirect effect is represented by a simple relationship in ALADIN-Climate relating the mass of hydrophilic aerosols to the cloud droplet number concentration (CDNC) based on the work of Martin et al. (1994). The radiative properties (COD, SSA and ASY) of liquid clouds are calculated in the SW spectral region by the parameterizations proposed by Slingo and Schrecker (1982). In the present work, we do not discuss possible first indirect effects between BBA and Sc which will be addressed and analyzed in a specific future companion study. The impact of aerosols on liquid clouds via the second indirect effect (precipitation modulation due to the hygroscopic aerosols) is currently under development. In these simulations, the autoconversion rate from water cloud to rain is not sensitive to the aerosol loading and the value of $8 \cdot 10^{-4} \text{ kg} \cdot \text{kg}^{-1}$ (Smith et al., 1990) is used for the critical cloud water mixing ratio.

3. Model Configuration and Data Used

3.1. Simulation Design and Important Physics Options

The ALADIN-Climate simulations cover the period from 01 August to 31 October 2016. The lateral boundary conditions are provided by ERA-INTERIM (Dee et al., 2011). The possible long-range transport of BBA is not forced at the lateral boundary conditions but rather a large domain (Latitude : -37.1°S to 09.4°N ; Longitude :-33.4°W to 45.4°E) is defined encompassing the main biomass-burning sources. The horizontal resolution of the model is 12 km with 91 vertical levels (from 1015 to 0.01 hPa). The land surface is treated using the SURFEX model (Masson et al.,

1000 2013). As detailed latter, we also use a spectral nudging method described in Radu et al. (2008). The
FMR (RRTM, ~~Mlawer et al., 1997~~) radiative transfer scheme is used to calculate the SW (LW)
radiation. Finally, it should be mentioned that the possible impact of BBA reducing the sea-surface
temperature (SST) is not treated here and the ALADIN-Climate model is used in a forced mode
configuration (~~with fixed SST~~). This possible impact of BBA is outside the scope of the present
1005 study.

~~As mentioned previously~~, the biomass-burning emissions from the CMIP6 inventory have been
used for BC, OC and sulfur gaseous SO₂. ~~These emissions are monthly-averaged, reconstructed for
the 1997–2015 period from the Global Fire Emissions Database version 4 with small fires
(GFED4s). The methology is described by van Marleet al. (2017). In this work, the ALADIN-
Climate simulation uses one of the lastest historical year (2014) for BC and OC emissions, which
cannot allow the model to reproduce precisely the daily aerosol variations especially when they are
controlled more by emissions than dynamical aspects. However, it should be noted that the AOD
anomaly for September 2014 compared to the 2008-2015 CAMS reanalyses period (Figure S1 in
Appendix), indicates moderate differences of about ~0.05-0.1. Additionally, Sayer et al. (2019)
found similar above-cloud and total-column AOD over the southern Atlantic Ocean in 2014 and
2016. These suggest that the effect of potential differences between 2014 and 2016 over the biomass
burning region is likely to be small. One of the interest of using such methology is to evaluate the
ALADIN-Climate model in its climate configuration, which will be exactly the same as used to
adress the radiative and climatic impact of BBA at climatic scale.~~

1010
1015

1020 Following the study of Petrenko et al. (2017), an adjustment factor of 2.5 is applied to the biomass
burning emissions. BBA are emitted into the first vertical level of the model, without any
considerations of pyroconvective processes, as no clear consensus on such processes exists over this
region. For example, Labonne et al. (2007) showed that smoke plumes are generally confined in the
planetary boundary layer (PBL) ~~close to the main biomass-burning source regions. Aeeordingly, In
the simulation, smoke emissions force the model at the first model level following the
recommendations from the first phase of AEROCOM (Dentener et al., 2006).~~ Fire emissions from
the savannah are emitted at the lowest model level, allowing subgrid-scale turbulence mixing
through the boundary layer. The diurnal cycle of smoke emission is not taken into account, which
could impact the temporal variations of the aerosol loadings (Xu et al., 2016). We assume that the
1030 main smoke emissions transported over SAO are included in the domain defined in Figure 1.
Finally, a climatology is used in the model for organic aerosols ~~produced~~ from vegetation biogenic
emission ~~and water vapor released from biomass combustion is not treated in the model.~~

The BBA mass is known to increase during aging due to the condensation of volatile organic compounds. In the absence of an explicit representation of secondary organic aerosols (SOA) production in ALADIN-Climate, a ratio of particulate organic matter (POM) to primary OC has been used for artificially representing SOA formation within the smoke plume, **when the mass is transferred from the fresh to aged mode in the model**. The lack of a complete representation of SOA in current climate models obviously represents an important source of uncertainties in the estimation of BBA concentration (Johnson et al., 2016). For this ALADIN-Climate simulation, an average POM/OC ratio of 2.3 is applied (Formenti et al., 2003) based on SAFARI-2000 data. This value is consistent with the recent results obtained by Vakkari et al. (2018) and higher than the one (1.6) retained in the HadGem global model (Bellouin et al., 2011, Johnson et al., 2016).

Regarding the large uncertainties related to the POM to OC ratio, two sensitivity tests using different POM to OC ratios (2 and 3) have been performed, showing an **important** impact of ± 0.15 on BBA AOD over the continent (Figure S2 in the supplement material). An additional simulation tested the sensitivity of BBA AOD to the e-folding time using the recent value proposed by Vakkari et al. (2018). The results (Figure S2 in Supplement Material) indicate a slight AOD decrease of about -0.05 when averaged over the box_S (15-25°E / 5-15°S, see Figure 1), **suggesting in this case a higher sensitivity of AOD to the choice of the POM to OC ratio**.

Three Four ALADIN-Climate simulations (excluding the sensitivity tests only shown in Figure S2, Supplement Material) are performed. The first one (control run, CTL) does not take BBA into account, while the second simulation (named SMK) includes the direct and semi-direct radiative effect of BBA. **As mentioned previously and as absorbing properties of smoke are fixed, the seasonal variations of smoke SSA during the biomass burning season as described in Eck et al. (2013) is not represented in the model. To address this limitation, a simulation (named SMK_SSA) has been performed using less absorbing smoke (SSA of 0.92 at 550 nm)**. Finally, a nudged (on wind and relative humidity) simulation (named SMK_SN) investigates more specifically the impact of the water vapor transported within the smoke plume on BBA optical properties and the associated SW radiative heating. For the latter, the nudging does not affect PBL, which can be independently influenced by the radiative effects of smoke.

3.2 Surface, Aircraft, Satellite and Reanalysis dataset

Different datasets of aerosol and cloud properties from surface, remote-sensing, and reanalysis, have been used for evaluating the ALADIN-Climate simulations. Satellite and reanalysis data are summarized in the Table 2.

1065 3.2.1. LASIC Surface Observations (Ascension Island)

SSA (at 529 nm) at Ascension Island was estimated from the in-situ measurement of the scattering coefficient estimated by a nephelometer and the absorption coefficient deduced from a Particle Soot Absorption Photometer (PSAP). The PSAP measurements incorporate an average of the Virkkula (2010) and Ogren (2010) wavelength-averaged corrections, and are collected at standard
1070 temperature and pressure, with dilution corrections applied. The RH of the air entering the PSAP is estimated to be 25% or less, while the air entering the nephelometer is measured, with values ranging between 45%-60%. Differences in the RH are speculated to bias the SSA higher rather than lower, because drying will reduce the coating thickness on the refractory black carbon, reducing lens-induced enhancement of shortwave absorption. The original nephelometer scattering
1075 measurements at 550 nm are converted to estimated values at 529 nm using the scattering-derived angstrom exponent. These measurements are also reported in Zuidema et al. (2018). An independent evaluation of the SSA in August-September 2017 using an Aerodyne Cavity Attenuated Phase Shift-SSA instrument is consistent with the values reported here (Tim Onasch, personal communication).

3.2.2. AERONET retrievals

1080 Two continental (**Mongu Inn** and Lubango) and one maritime (Ascension Island) AERONET sites extend local comparisons to the atmospheric column and for different aerosol variables. As described by Dubovik and King (2000), the AERONET network allows retrieval of microphysical (volume size distribution) and optical (refractive indexes, SSA, ASY and scattering/absorption optical depth) properties of aerosols, as well as their spectral dependence in SW spectral range. The
1085 uncertainty of retrieved SSA is ± 0.03 for AOD (440 nm) > 0.2 for water soluble aerosols and for AOD (440 nm) > 0.5 (zenith angle larger than 50 degrees) for desert dust and BBA. For AOD (440 nm) < 0.2 , the SSA accuracy is ± 0.05 – 0.07 (Dubovik et al., 2000). **In this study, we focus our analyses on Level 2 AOD and SSA AERONET products from AERONET version 2.**

3.2.3 Aircraft Observations

1090 3.2.3.1 Aerosol Extinction profiles

The NASA Langley 2nd generation High Spectral Resolution Lidar (HSRL-2) has been in operation during ORACLES-1 aboard the NASA ER2. HSRL-2 measures particulate backscatter and extinction at 355 nm and 532 nm using the HSRL technique (Shiple et al., 1983) and aerosol backscatter at 1064 nm. All three wavelengths also measure depolarization. The HSRL technique
1095 uses a separate filtered channel at each HSRL wavelength that is sensitive to molecular scattering, but not aerosol scattering. **This channel therefore provides a direct observation of the attenuation of the signal and allows for the direct calculation of aerosol extinction without external constraints or assumptions on the aerosol optical depth or lidar ratio. ~~and which therefore provides with a direct observation of the attenuation of the signal.~~** From this, the vertically-resolved particulate extinction

1100 is derived by comparison to a molecular density profile from direct measurement or a model. For
ORACLES-1, the HSRL-2 retrieval uses molecular density profiles from MERRA2 (Gelaro et al.
2017). The filtering is accomplished with an iodine gas filter at 532 nm (Hair et al. 2008) and a
density-tuned field-widened Michelson interferometer at 355 nm (Burton et al. 2018). More
information about the instrument, calibrations, and algorithms is given by Hair et al. (2008) and
1105 Burton et al. (2015, 2018). The vertical resolution for extinction is 315 m and for backscatter and
depolarization is 15 m. The horizontal resolution is 60 seconds for extinction and 10 seconds for
backscatter and depolarization, or approximately 10 km (extinction) and 1.8 km (backscatter). The
ORACLES HSRL-2 extinction product can be found at
<https://espoarchive.nasa.gov/archive/browse/oracles/id8/ER2>.

1110 3.2.3.2 SW Heating Rate estimates

Heating rate profiles segregated by absorber (aerosols, water vapor, oxygen) are determined using
the spectral information from the Solar Spectral Flux Radiometer (SSFR). SSFR measures
upwelling (nadir) and downwelling (zenith) irradiance from 350-2100 nm. The zenith light collector
is actively leveled, which allows SSFR to obtain spectral irradiance measurements throughout spiral
1115 profiles that extend from the top of the aerosol layer to the bottom of the cloud layer. These
measurements lend themselves to a new algorithm for retrieving aerosol SSA and ASY from 350-
860 nm. It uses measurements made during the spiral aircraft descents to separate changes in
upwelling, downwelling and net irradiance due to the aerosol layer from those due to the underlying
cloud field (Cochrane et al., 2018).

1120 The 4STAR spectral AOD, HSRL-2 extinction profiles, and the spectral SSA and ASY retrievals,
provide the inputs for the heating rate profiles calculated with the LibRadtran radiative transfer tool
(Mayer and Kylling, 2005). The retrieved intensive aerosol properties SSA and ASY are vertically
homogeneous, whereas the spectral extinction coefficient from the merged 4STAR HSRL-2
measurements varies with altitude. The cloud albedo below the aerosol layer is directly measured
1125 by SSFR (the reflectance has been estimated around ~ 800 m above cloud top), and the atmospheric
water vapor profile is determined from in situ measurements. Using these inputs, two calculations
of the heating rate profile are done: one with, and one without aerosols, and the difference is
reported as aerosol heating rate. The accuracy of the calculation is ensured by comparing the
calculated irradiance spectrum above and below the aerosol layer with the SSFR measurements.
1130 After this step, the heating rate is spectrally integrated over the solar wavelength range (380-2125
nm).

3.2.4 Satellite Retrievals

3.2.4.1 MODIS and MISR dataset

The Deep Blue ACAOD retrieved from the MODIS instruments is described in Sayer et al. (2019),
1135 which is a slightly updated version of the demonstration algorithm presented in Sayer et al. (2016).
In brief, this algorithm performs a multispectral weighted least-squares fit of measured reflectance
in four bands across the visible spectral region (centered near 470, 550, 650, and 870 nm) to
simultaneously retrieve ACAOD and the COD. The minimization is performed using optimal
estimation. This provides estimates of the uncertainty on retrieved parameters, as well as an
1140 indicator of how well the retrieval solution is able to fit the measurements. Retrievals where the
forward model is expected to be inappropriate, or where the measurements do not constrain the
retrieved quantities, are filtered out.

The main updates since Sayer et al (2016) are twofold. First, the radiative transfer lookup tables
have been updated to include dimensions for surface pressure and surface albedo, which improves
1145 the realism of the forward model over land. Surface pressure is estimated using terrain altitude,
while the surface albedo is taken from a climatology based on the MODIS gap-filled snow-free land
albedo data set (Sun et al., 2017). The second is that, rather than applying the retrieval to each
individual pixel, the pixels are aggregated into 10 km x10 km (effective nadir resolution) boxes,
chosen to match the resolution of the level 2 MODIS aerosol products. Then, the median reflectance
1150 of water cloud pixels within each box is used for the retrieval. Use of median reflectance decreases
sensitivity to factors such as 3D effects or cloud detection errors. Additionally, if a 10 km x 10 km
pixel has a water cloud fraction under 0.75, it is excluded, for the same reason.

The MOD06ACAERO (Meyer et al., 2015) products are also used. These use reflectance
observations at 6 MODIS spectral channels (0.46, 0.55, 0.66, 0.86, 1.24, and 2.1 μm) to
1155 simultaneously retrieve ACAOD, and the COD and the cloud effective radius (CER) of the
underlying marine boundary layer clouds. Retrievals are performed at the pixel level (here, every
fifth native 1 km pixel) on both Terra (morning) and Aqua (afternoon) MODIS data. Output
includes pixel-level estimates of retrieval uncertainty that accounts for known and quantifiable error
sources (e.g., radiometry, atmospheric profiles, cloud and aerosol radiative models). Assumptions
1160 regarding the cloud forward model and ancillary data usage are consistent with those of the
operational MODIS cloud products (MOD/MYD06) (Platnick et al., 2017). Note that both these
data sets represent only the partial column AOD, i.e. the AOD above the liquid cloud top, and that
ice phase clouds are not processed. In addition, we have also used MODIS-Terra and Aqua
combined Deep Blue/Dark Target data set
1165 (AOD_550_Dark_Target_Deep_Blue_Combined_Mean_Mean) from the latest Collection 6.1
(Sayer et al., 2014) and MISR (MIL3MAE monthly mean data at 0.5° of resolution; Kahn et al.,
2015) (see Table 2).

3.2.4.2 OMI dataset

The Ozone Monitoring Instrument (OMI) sensor, operating since October 2004 onboard of the EOS
1170 Aura satellite, is a spectrometer with a high spectral resolution (Levelt et al., 2006). OMI offers
nearly the daily global coverage with a spatial resolution for the UV-2 and VIS (UV-1) channels
ranging from $13 \times 24 \text{ km}^2$ at nadir. The OMAERUV_v003 product contains retrievals from the
OMI near-UV algorithm (Torres et al., 2007). This algorithm derives a variety of aerosol radiative
properties, such as an aerosol index (AI), AOD, AAOD (uncertainty of $\pm (0.05 + 30\%)$) for clear-
1175 sky conditions. For this study, we have used ACAOD (Jethva et al., 2018) retrieved at 500 nm
(Table 2). An above-cloud aerosol retrieval technique was also applied to the multi-year record of
OMI observations to deduce a global product of ACAOD on a daily scale (Jethva et al., 2018).

3.2.4.3. SEVIRI dataset

Spatiotemporally highly resolved geostationary satellite observations are taken here from the
1180 CCloud property dAtAset based on SEVIRI edition 2 (CLAAS-2, Benas et al., 2017). The CLAAS-2
dataset is based on measurements of the Spinning Enhanced Visible and Infrared Imager (SEVIRI)
and was generated and released by the EUMETSAT Satellite Application Facility on Climate
Monitoring (CM SAF) as the successor of CLAAS (Stengel et al., 2014). CLAAS-2 includes a
variety of cloud properties, of which LWP, COD and CER were used in this study. CLAAS-2 COD
1185 and CER are retrieved, similarly to the widely used cloud retrieval method described in Nakajima
and King (1990), under the assumption of plane-parallel cloud layers. Lookup tables are pre-
calculated and used to map SEVIRI reflectance at $0.6 \mu\text{m}$ and $1.6 \mu\text{m}$ wavelengths to COD and
CER as function of satellite-sun geometries and cloud phase. For liquid clouds, COD and CER are
used to calculate LWP following Stephens (1978). The algorithm is initially described in Roebeling
1190 et al. (2006) with more details and updates given in Benas et al. (2017), which also report validation
exercises. The CLAAS-2 Level-2 data are instantaneous data on native SEVIRI resolution with a
temporal resolution of 15 minutes. For this study, the data are projected onto a regular latitude-
longitude grid using nearest neighbor approach. **It should be noted that Sc cloud retrievals could be
affected by the presence of BBA over SAO. Recently, Seethala et al. (2018) indicate that, in the
1195 aerosol-affected months of July–August–September, SEVIRI LWP (based on the $1.6\mu\text{m}$ CER) is
biased by $\sim 16\%$.**

3.2.5. Reanalyses of atmospheric composition

Two different reanalyses are used for aerosols and clouds (Table 2). The European Center for
Medium-Range Weather Forecasts (ECMWF) reanalysis of global atmospheric composition since
1200 2003 includes five main aerosol species. The first generation of ECMWF reanalysis (Morcrette et
al., 2009), issued by the GEMS (Global and regional Earth-System (atmosphere) Monitoring using

Satellite and in situ data) project, covers the period 2003-2008. The Monitoring Atmospheric Composition and Climate (MACC) is the second-generation product and provides improvements in sulfate distributions and has extended to the 2003-2011 period (Benedetti et al., 2009). Here, we use
1205 MACC NRT daily data sets at 1.125° resolution of the anthropogenic SW direct forcing at TOA in all-sky conditions (Table 2). In addition, we use the Modern-Era Retrospective Analysis for Research and Applications (MERRA2) reanalysis, generated with version 5.2.0 of the Goddard Earth Observing System (GEOS) atmospheric model and data assimilation system (DAS). The system, the input data streams and their sources, and the observation and background error statistics
1210 are fully documented in Rienecker et al. (2011). We rely on the AOD for the different species at 0.5° × 0.625° spatial resolution (Table 2).

4. Microphysical and Optical properties of Sc and BBA

4.1. Sc properties

The different properties of Sc are analysed over the box 10-20°S / 0-10°E, defined by Klein and
1215 Hartmann (1993), referenced in the following as box_O.

4.1.1. Macrophysical and Microphysical Sc properties

Figure 2a reports the daily mean LWP (g.m⁻²), LCF as well as liquid COD, averaged over the box_O for September 2016. A reasonable agreement is evident in the LWP between ALADIN-Climate (SMK simulation), SEVIRI and ERA-INT data. The simulated LWP is in the range of ERA-INT and SEVIRI data, if slightly less, by -8 g.m⁻² in the mean compared to ERA-INT. The LWP maxima
1220 are also well simulated, especially for the 25-28 September, with LWP ~90 g.m⁻². The temporal correlation is about ~0.45 between ERA-INT and the SEVIRI LWP.

In contrast, an important negative bias of approximately ~-20% is detected in the simulated low cloud fraction compared to ERA-INT values (Fig. 2b). This result is related to a well-known ~~«too~~
1225 ~~few, too bright»~~ bias (underestimates of low cloud fraction) detected in most GCMs over the Sc regions (Nam et al., 2012). The mean modeled LCF is 57%, compared to 80% in the ERA-INT dataset. The poor representation of LCF over Sc regions remains an open issue outside of the scope of this work. Nevertheless, the analysis and discussions of the following results take into account this underestimates, notably for SW heating rate and the DRF exerted by BBA at TOA.

4.1.2. Optical Sc properties

Figure 2c represents the daily COD estimated by ALADIN-Climate using the Slingo et al. (1998) and Nielsen et al. (2015) parameterizations, which are used to calculate liquid cloud optical
1235 properties at different wavelengths from LWP and CER and different spectral coefficients. This figure also includes an ALADIN-Climate simulation with a fixed CER of 10 μm, close to the SEVIRI values (Figure S3 in Supplemental Material). Retrieved values from MODIS and SEVIRI

are also reported in Figure 2c. The SEVIRI and MODIS-Aqua values are consistent with each other, for a mean COD of ~ 8 for both instruments. The COD is overestimated by the model in both configurations but especially when the Slingo parameterization is used (average COD value of 11.5). The Nielsen parametrization slightly reduces the bias for a mean COD of 9.5. As the LWP is realistically simulated by the model, this negative bias could be due to errors (underestimates) in the simulated CER by ALADIN-Climate. Our sensitivity test conducted using a fixed CER of $10 \mu\text{m}$ indicates a reduced bias (+0.25). As mentioned previously, the BBA indirect radiative effect is not addressed in this study but is known to be an important issue over SAO (Costantino and Bréon, 2013, Lu et al., 2017). **The indirect radiative effect is also relevant to DRF as it strongly depends on the albedo of the underlying Sc.** The impact of BBA on cloud microphysical properties will be studied in a future work.

4.2. Biomass Burning Aerosols

4.2.1. AOD over biomass burning source

Figure 3 compares the (monthly mean) total (clear-sky, not above-cloud) AOD simulated by ALADIN-Climate to those derived from MODIS-Terra and Aqua combined Deep Blue/Dark Target data set (AOD_550_Dark_Target_Deep_Blue_Combined_Mean_Mean) from the latest Collection 6.1 (Sayer et al., 2014) and MISR. The total AOD obtained from the MERRA2 and CAMS reanalyses are also indicated. All AODs are at 550 nm. Over Angola and Zambia, the model is able to simulate a regional pattern of AOD consistent with the MODIS and MISR retrievals, with AODs of $\sim 0.7-0.9$, even if BBA are located too far south compared to satellite data. **A general good agreement is also observed compared to the CAMS reanalyses, even if the model underestimates AOD over eastern Gabon.** Over the continent, significant differences (overestimates) appear clearly compared to MERRA2. This difference with reanalyses product can be due to the scaling factors applied for biomass burning emissions in the different models. Over the ocean, ALADIN-Climate is found to be very consistent with MERRA2 (AOD ~ 0.7 near the Angola coast) but the differences are large compared to the satellite retrievals. The latter AODs are higher ($\sim 0.7-1.0$), especially for MODIS. It should be mentioned that 50% of MODIS AOD over the SAO is due to coarse mode according the level 2 retrievals.

In addition, the land-ocean contrast in AOD detected by MODIS and MISR, with lower AODs over the continent and higher AODs over the ocean, is not observed in ALADIN-Climate. This contrast in AOD is still detected in MERRA2 data, but it is not as large as in the satellite retrievals. It is likely that some of the land/ocean contrast in the satellite data comes from **two different** factors. The first is that the over-land and over-water algorithms are different and may have different biases. The second is that cloud fraction is also significantly higher over the water than over the land, meaning

1270 that typically more days of data contribute to the monthly mean over land than over water. Both of
these effects could suppress or enhance any real land-ocean contrast in the AOD. **Finally, part of the
contrast could be due to the presence of sea-spray aerosols, certainly about ~0.1.** As well as
continued refinement of AOD retrieval algorithms, it is recommended that future work attempts to
1275 quantify the potential magnitude of these sampling effects on land/ocean contrast, which have
received comparatively little attention to date. Finally, the satellite data also indicate a larger spatial
extent to the aerosol loading over the ocean compared to ALADIN-Climate. This difference could
be due to possible overactive aerosol deposition in our simulations. A specific section (4.2.2) is
dedicated to using ACAOD products for evaluating the model over the ocean.

In order to make ~~more-robust~~ comparisons over the continent, a second box (box_S, 15-25°E / 5-
1280 15°S, see Figure 1) is defined over biomass burning sources. Figure 4a indicates the daily-mean
AOD at 550 nm averaged over box_S from MODIS, MERRA2 and ALADIN-Climate. There is a
good agreement, with monthly means of 0.59, 0.62 and 0.49 for MODIS, ALADIN-Climate and
MERRA2, respectively. The model is very consistent with the MODIS retrievals and slightly higher
than MERRA2. Differences between MERRA2 and ALADIN-Climate may reflect the different
1285 model biomass burning emissions. Compared to MODIS, a small mean bias of +0.04 is found in the
model over smoke sources. In terms of temporal correlation, the score is worse compared to
MODIS. **As mentioned previously,** this could be due to the time frequency of biomass burning
emission (**monthly-mean emission**) imposed in the ALADIN-Climate model. The absence of
spectral nudging in the ALADIN-Climate simulation can also explain part of the low temporal
1290 correlation, which is clearly higher (0.73) for MERRA2 data.

Data from three AERONET stations (Mongu (Zambia), Lubango (Angola) and Ascension Island)
provide additional AOD evaluation. Figure 5 indicates the daily-mean AERONET and ALADIN-
Climate (only daytime values) AOD at each station. At Lubango, the model is able to correctly
simulate the AOD, except in the beginning of September when it is overestimated. The maxima
1295 (AOD of 0.6) of 20 and 27 September are also well represented by the model. The total monthly-
mean AOD simulated by ALADIN-Climate (0.41) is consistent with AERONET (0.43), if with a
small mean negative bias. Over the Mongu station, the comparisons indicate a more pronounced
negative bias (mean value of -0.14). This is due to a nearly constant underestimate of total AOD
throughout the period of the simulation, leading to a simulated monthly-mean of 0.47, lower than
1300 the one observed (0.61). In parallel, the two maxima detected in AERONET data are well captured
by the model. The first one, occurring between the 18 and the 21 September, is simulated too early
and its magnitude is overestimated by about ~0.2. The second (23-29 September) is better
reproduced in terms of magnitude (~ 1.0) but a significant underestimate in its duration is observed.

Indeed, the BBA event starts around the 22 September in the observations, while it is simulated
1305 between 26 and 29 September by the model. Finally, the model is able to correctly simulate the
magnitude of AOD along the transport over SAO to the remote location of Ascension Island (Figure
5). The simulated monthly-mean value (0.26) is comparable to AERONET (0.21) with a small
positive bias, primarily because of overestimates during the 06-10 September period. This suggests
that winds and aerosol deposition are also well represented. To summarize, the analysis of AOD
1310 comparisons demonstrate that the ALADIN-Climate model reasonably simulates the magnitude of
AOD during September 2016, even if some biases are detected (possibly due to the monthly-mean
emissions imposed in the model that do not allow the model to represent some daily variations
precisely), especially over the ocean (a negative bias, primarily near the coast) when compared to
satellite data.

1315 4.2.2 ACAOD over SAO

Due to the significant presence of Sc over SAO, the use of satellite clear-sky AOD products as a
model evaluation tool is limited. This limitation is overcome with new retrievals of ACAOD from
MODIS and OMI, summarized in Table 2. Figure 6 indicates consistent estimates of monthly-mean
ACAOD between ALADIN-Climate, MODIS-DB, MOD06ACAERO and OMI. It should be noted
1320 that the ACAOD is calculated as the integration of the aerosol extinction from the cloud top to the
model top in the ALADIN-Climate model. For all independent estimates, Figure 6 indicates values
of about ~0.4-0.5 (550 nm) near the Angola coast. ACAOD then decreases to ~0.2 over SAO.
ACAOD is underestimated by ALADIN-Climate over the ocean, especially when compared to the
two different MODIS products. Indeed, MODIS-DB and MOD06ACAERO data reveal a larger
1325 regional extent over the ocean compared to the model. The ACAOD extent is less pronounced in the
OMI data, which is thereby more consistent with ALADIN-Climate.

Additional comparisons were performed over box_O using MODIS-DB products. Figure 4b
indicates daily-mean model ACOAD obtained for the SMK and SMK_SN (not discussed in this
part) simulations and MODIS-DB. The monthly-mean ACAOD is underestimated by the model
1330 (SMK configuration, red dotted line) with a mean value of 0.20 (at 550 nm), 0.06 less than MODIS-
DB (0.26). The ALADIN-Climate simulation underestimates two maxima observed by MODIS-DB,
around 03-05 and 20-24 of September, explaining part of the negative bias (-0.06) in the SMK
simulation. For the rest of the time period, we observe a realistic estimation of ACAOD by the
model. It should be mentioned that additional analyses of the simulated ACAOD is also discussed in
1335 Shinozuka et al. (2018) for different boxes defined in the ORACLES-1 program, indicating similar
results with an underestimate of ACAOD. As for AOD, ALADIN-Climate is shown here to simulate
realistically the concentration of aerosols transported above clouds over SAO. This allows to

address the SW DRF exerted by BBA at TOA during ORACLES, after investigating the vertical structure (part 4.2.3) and SW absorbing properties (part 4.2.4).

1340 4.2.3 BBA Vertical Structure

4.2.3.1 ALADIN-Climate Extinction vertical profiles

The vertical distribution of the modeled BBA extinction is analyzed over the continent and SAO in Figure 7 as the monthly-mean extinction vertical profiles (at 550 nm) for two different transects at latitudes of 8 and 15°S. For both transects, the highest extinctions are identified over the continent, close to biomass burning sources, with extinctions $\sim 0.2 \text{ km}^{-1}$. The amplitude of BBA extinction coefficient (top and bottom right panels) decreases during the transport, reaching values of $\sim 0.05\text{-}0.10 \text{ km}^{-1}$ (at 8 and 15°S, respectively) for longitudes near 0°. For both profiles, the top of the smoke plume is around $\sim 5000 \text{ m}$ over the continent in the simulations, very consistent with the altitude of the top plume over the continent reported by Das et al. (2017) from CALIOP lidar observations. **This analysis would suggest that injection heights are not that important in this region and aerosols are mainly lofted by convection over the biomass burning sources.**

Over the SAO, two different well-distinguished aerosol layers are simulated ; a first one mainly located in the MBL and mostly due to primary sea spray aerosols and a second BBA layer located above, between 2000 and 4000 m. The top of the marine aerosol plume is simulated around $\sim 1000 \text{ m}$ in the model and is separated from the smoky layer by a clean atmospheric layer, especially at 15°S, characterized by extinction near $\sim 0.05 \text{ km}^{-1}$. For both transects, the top of the smoke plume decreases from 10°E to 10°W, starting around $\sim 5000 \text{ m}$ near the coast to reach $\sim 4000 \text{ m}$ at 10°W. This BBA stratification over SAO is consistent with the vertical structure reported by Das et al. (2017) for latitudes comprised between 0 and 10°S. Indeed, they report a transport of smoke that mainly occurs between 2000 and 4000 m over SAO, contrary to the different models used in this study, which both indicate a more pronounced decline of the altitude of BBA during the transport. This result is also consistent with a previous study from Haywood et al. (2003) over this region.

The elevated plume is mainly composed by BBA characterized by a decrease in extinction (**mainly due to a decrease of BBA concentration**) during the transport from 0.15 km^{-1} (at 15°E) to 0.08 km^{-1} (near 0°) for the transect at 8°S. Such extinction values are consistent with those reported by Das et al. (2017), who indicated CALIOP extinction around $\sim 0.1\text{-}0.15 \text{ km}^{-1}$ over SAO (for latitudes between 0 and 10°S). The extinction due to BBA is negligible in the simulation for longitudes highest than $\sim 10^\circ\text{W}$, especially for the transect at 15°S. For both transects reported in the Figure 7 (left panels), significant extinctions are simulated within the MBL, with values of about $\sim 0.2\text{-}0.25 \text{ km}^{-1}$ mostly due to the presence of primary sea-spray aerosols. Figure 7 indicates the highest values at 8°S compared to 15°S.

Based on the transects, no favorable conditions are identified allowing an efficient mixing of BBA within the MBL during the transport of aerosols over SAO. Such results are ~~contradictory found to be different~~ to the schematic view of Gordon et al. (2018), who proposed that an efficient mixing of smoke only occurs around 0° E - 10° W within the MBL. ~~Advections processes are absent in our simulations and~~ This could limit the possible impact of BBA on cloud droplet concentrations and Sc properties. In the ALADIN-Climate simulations, smoke aerosols primarily remain above the MBL during transport, with little vertical mixing. For this reason, in the model, the impact of BBA on the Sc microphysical/optical properties will be primarily through the semi-direct radiative effect.

1380 4.2.3.2 Comparison with HSRL-2 Extinction

Aerosol extinction coefficients derived at three different wavelengths (355, 532 and 1064 nm) by the HSRL-2 instrument permit local 1-D comparisons with ALADIN-Climate simulations. In addition to evaluating the simulated extinction vertical profiles, the spectral dependence of the model calculated extinction can also be evaluated. Figure 8 reports the extinction vertical profiles for three different days (12, 22 and 24 September), as well as RH profiles obtained from MERRA2 and ALADIN-Climate (black dotted and solid lines, respectively). Those specific days have been chosen to represent different locations within Box_O (Figure 1). The vertical profile of CF simulated by ALADIN-Climate (yellow dotted line) is also included in Figure 8. It should be mentioned that the wavelengths of ALADIN-Climate are not exactly the same as those from HSRL-2, especially for the UV spectral band (355 and 440 nm, respectively). In addition and due to the significant CF, HSRL-2 data are not necessarily available near the surface and remain above cloud top (~2000 m) in most cases.

For September 12, our simulations indicate that the vertical structure of the BBA plume (dashed red, purple and blue lines) is not well represented in the model even though both the model and HSRL-2 place most of aerosol above the MBL. At both times (11:00 and 13:00 UTC), the aerosol extinction coefficients simulated by ALADIN-Climate are overestimated (underestimated) for altitudes between 1500-3000 m (3000-6000 m). This compensation of errors leads to a consistent averaged (between 1500 and 6000 m) integrated extinction in the simulation (0.07 km^{-1} at 550 nm) compared to HSRL-2 observations (0.06 km^{-1}) at 13:00 UTC but significant underestimates at 11:00 UTC (0.05 and 0.13 km^{-1} , for ALADIN-Climate and HSRL-2, respectively). In addition, we observe important biases in the simulated RH, especially at 11:00 UTC between the surface and 3000 m (positive bias) and (negative bias) above 3000 m, ~~which could partly explain the extinction biases~~.

For the 22 and 24 September, Figure 8 indicates that the altitude of the smoke plume over SAO is realistically represented by ALADIN-Climate, especially for the plume located between 3000 and 6000 m. However, a second aerosol layer, which is observed from HSRL-2 between 2000 and 3000

m for September 24 at 11:00 UTC (Figure 8e) is absent in ALADIN-Climate and simulated below (between 1000 and 2000 m). For the same day at 12:00 UTC (Figure 8f), similar conclusions are obtained with a maxima at ~3500 m which is well simulated by ALADIN-Climate but the second plume (observed around ~2000-2500 m from HSRL-2) is totally absent in the model. For both days, Figure 8 reveals that the magnitude of the simulated extinction is generally underestimated compared to HSRL-2, true at each wavelength. As an example, for 24/09 at 11:00 UTC (Figure 8a), the local maxima (~0.30 km⁻¹) derived by the HSRL-2 instrument at 5000 m is significantly lower (~0.15 km⁻¹) in the model. This is also observed for the second aerosol plume at ~2500 m for that day. Such conclusions can be drawn for all cases (12, 24 and 26 of September), with a negative (mean) bias (indicated only at 550 nm and for the whole atmospheric column) of between -0.01 and -0.08 km⁻¹. This could be attributed to incorrect smoke emissions, e-folding time, OC to POM ratio, optical properties (especially the mass extinction efficiencies) of BBA, as well as the different parameterizations used for representing hygroscopic properties of aged smoke. In section 4.3, specific attention is paid to the impact of RH transported within the smoke plume on BBA extinctions.

4.2.4 BBA (SW) Absorbing properties and Heating rate

4.2.4.1 Absorbing properties at the biomass burning source

The magnitude and the sign of the DRF of BBA exerted over SAO is highly sensitive to the smoke SSA. The monthly-mean (whole-column integrated) SSA (for the fine aerosols) simulated by ALADIN-Climate for September 2016 (Figure S4 in Supplement) indicates values of about ~0.85 (at 550 nm) over a large part of the subcontinent. SSA increases near the coast (~0.89-0.90) and during transport over the SAO (~0.92 to 0.95). Local comparisons at the two continental AERONET stations (Mongu and Lubango, Figure S4 in Supplement) reveal a good agreement between the simulated and observed SSA, characterized by low bias of about +0.01/-0.02. A larger negative bias is observed and documented at the Lubango site. However, the day to day variability is not represented in the model and SSA is nearly constant (~0.83-0.84) in the simulation. As an example, the lowest values (~0.79-0.80 ± 0.04) detected by AERONET are absent in the model. The same conclusion is obtained for the highest values derived from observations, especially at Lubango (Figure S4 in Supplement). However, such results indicate the ability of the model at reproducing absorbing properties of BBA close to biomass burning emissions with limited bias (-0.02/+0.01).

4.2.4.2 Absorbing properties over SAO

The model comparison to in-situ surface-based SSA values at Ascension Island reveals more discrepancy. Figure 9 shows the daily-mean SSA obtained at the surface from in-situ observations

1440 and calculated with ALADIN-Climate at two different altitudes (0.2 and 3 km). The model is not
able to reproduce the low values (mean of 0.87) observed at the surface. Indeed, near the surface,
the simulation indicates a simulated SSA of nearly 1 for all of the September 2016 period. The
model MBL optical properties are mainly controlled by primary marine aerosols (see Figure 7)
leading to SSA close to unity. This highlights also that the mixing of BBA within the MBL is
1445 possibly underestimated in the model, although LASIC observations also show little smoke is
present at the surface in September (Zuidema et al., 2018). **The LASIC site is also located on the
remote windward side of the island and is not affected by local sources, of which there are few to
begin with (no trash burning on the island).**

It should be noted that the low values of SSA obtained at Ascension island **could** reflect long-term
1450 ageing processes for the BBA that are not currently included in ALADIN-Climate. **One indication
that the aerosol sampled at the LASIC is aged is through the parameters f44 and f60 (the fraction of
the organic aerosol mass spectrum signal at m/z 44 and 60 respectively), in the data from the
Aerosol Chemical Species Monitor (Alison Aiken, personal communication). The LASIC f44 and
f60 values of approximately 0.2 and 0.002 respectively are characteristic of highly aged aerosols**
1455 **(Cubison et al., 2011). This chemical process could increase the absorbing efficiencies of BBA
(Fierce et al., 2016) due to the « lensing » effect (increase of SW radiations reflected to the
absorbing core) during the transport (decrease of SSA) and could explain the opposite results
obtained in the model, which simulates an increase of SSA (not shown, Figure S4) from biomass
burning sources to SAO.**

1460 4.2.4.3 SW Heating Rate

Figure 10 indicates the SW heating rates only due to BBA for two transects defined at latitudes of 8
and 15°S, similar to Fig. 8. The effect of BBA is isolated by subtracting the heating rates in the
simulations without BBA from those with BBA. Significant additional SW heating is simulated
over the continent and between 2 and 4 km over SAO due to the presence of absorbing smoke. Over
1465 the continent, the additional heating is about ~1 °K by day with maxima near ~1.5 °K by day for
altitude of ~4000m at 8°S. The simulated heating is approximately 1°K/day near the coast,
decreasing to 0.5°K/day during transport. For both transects, SW heating occurs mainly between 2
and 4 km over SAO. At 15°S, the SW heating is less pronounced than at 8°S, in agreement with the
difference in the extinction profiles (see Fig. 7). The SW heating due to BBA absorption is clearly
1470 visible only above the MBL and there is no clear additional SW heating within it.

Such values of SW heating due to smoke appear to fall well within the range of values reported **by
different modeling studies by** Tummon et al. (2010), Gordon et al. (2018), Adebisi et al., (2015) or
Wilcox et al. (2010), who reported, respectively, additional SW heating due to smoke of 1 (JJAS

period), 0.34 (5 days of simulations), 1.2 (for fine AOD > 0.2) and 1.5 °K by day. In addition, Keil
1475 and Haywood (2003) estimated a SW heating rate of 1.8°K/day near the coast using a radiative
transfer model and observations during SAFARI-2000. The temperature change (estimated through
two parallel simulations including or not smoke) due to BBA is about +0.5-0.8 °K between 2 and 4
km (Figure S5 in Supplement material) in a good agreement with the value (+0.5 °K) of Sakaeda et
al. (2011) or more recently proposed by Gordon et al. (2018). **It should be noted the large impact of
1480 less absorbing BBA (mostly present at the end of the biomass burning season, Eck et al., 2013) on
SW heating rate as reported in Table 3. Results obtained with the SMK_SSA simulations indicate a
change from 1.15°K/day (SMK) to 0.58°K/day (SMK_SSA) over the box_S.**

ORACLES SW heating rates retrieved from the SSFR retrievals of SSA and ASY (see Part 3.2.3.2)
in conjunction with HSRL2 extinction profiles (Part 3.2.3.1) are also used to assess our simulations.
1485 Figure 11 indicates the instantaneous (12:00 UTC) SW heating (only due to aerosols) vertical
profiles obtained for 20 September from SSFR and ALADIN-Climate. Two ALADIN-Climate
heating profiles indicate clear-sky and all-sky conditions. Figure 11 indicates that the location of the
additional SW heating due to BBA is well represented by the model, with a notable increase
between 3 and 4 km, in agreement with the SSFR retrievals. SW Heating between 2 and 2.5 °K/day
1490 are simulated at these altitudes with the highest values obtained under all-sky conditions (black
dashed lines). However, significant underestimates are observed within the smoke layer, where
SSFR observations indicate SW heating of about ~3 to 3.5 °K/ day. As the Sc COD is found to be
consistent between simulations and the SSFR cloud retrievals (COD ~9), we hypothesize that the
difference in SW heating is due to local underestimates of aerosol extinction as well as of BBA
1495 absorption in the model. A second aspect concerns the large underestimate of SW heating around
~1.5 km in the ALADIN-Climate simulation. Indeed, the local maxima of ~2.5 °K/ day obtained
from SSFR observations is totally absent in the model, but can be traced back to another layer
detected by HSRL.

4.3 Impact of the RH transported within the smoke plume on optical properties

1500 As mentioned previously, a specific simulation (SMK_SN) that includes the method of spectral
nudging (Radu et al. 2008) was also performed. The nudging is applied to wind vorticity and
divergence, surface pressure, temperature and specific humidity, using a constant rate above 700
hPa, a relaxation zone between 700 and 850 hPa, while the levels below 850 hPa are free. This
simulation was motivated by different studies (Haywood et al., 2003, Adebisi et al., 2015) that
1505 indicated a correlation between BBA and specific humidity. In these studies, biomass burning
plumes are associated with specific humidities greater than 2 g.kg⁻¹, while outside the smoke
plumes the values are less than 1 g.kg⁻¹. To date, few regional climate modeling studies have

investigated the ~~humidity's~~ potential role of the relative humidity on smoke optical properties within this specific atmospheric layer, that could, in turn, impact the DRF exerted by BBA. This
1510 ALADIN-Climate simulation (SMK_SN) addresses this specific point.

Figure 4b showing the daily-mean ACAOD (averaged over the box_O) from MODIS-DB along with the simulations through comparing the ACAOD with and without the nudging of RH, indicates an impact. For SMK_SN, the negative bias is reduced compared to MODIS-DB and equals to -0.02 (bias of -0.06 for the SMK run). The maxima in ACAOD observed between 19 and 25 September
1515 is better reproduced in the SMK_SN simulation, consistent with a slightly improved temporal correlation (0.42).

In addition to the satellite observations, we also used HSRL-2 vertical profiles of extinction (already presented in Figure 8) to investigate the impact of RH on BBA optical properties. Figure 12 shows, for 24 September only, the vertical profiles of RH by MERRA2 and ALADIN-Climate
1520 (SMK and SMK_SN simulations), as well as aerosol extinction (at 550 nm) from HSRL-2 and the model (SMK and SMK_SN). A significant improvement is evident in the SMK_SN RH vertical profiles, reducing the bias with MERRA2, especially at 09:00 and 12:00 UTC. For each case, Figure 12 indicates that RH is better represented in SMK_SN especially at altitudes where the transport of smoke occurs, i.e., between 2000 and 5000 m (Figure 7).

These changes in RH profiles in SMK_SN run impact the BBA optical properties for the different cases, notably by increasing extinction within the smoke plume and a remarkable agreement in extinction is observed between HSRL-2 and the SMK_SN simulation. As an example, at 09:00 UTC, the improvement of the simulated RH between 3500 and 6000 m in SMK_SN significantly reduces the bias in the simulated extinction at those altitudes. At 4500 m, the simulated extinction is
1530 very consistent with HSRL-2, with maxima around $\sim 0.2 \text{ km}^{-1}$. Similar conclusions are also observed for the other cases presented in Figure 12. At 11:00 UTC, important improvements are found for altitudes between 2000 and 5000 m in the SMK_SN simulation compared to SMK. At this time, a negative bias persists between 2000 and 3500 m, marked by a bias in RH even in the nudged simulation. These results are consistent with the study of Adebisi et al. (2015) who used CALIPSO
1535 smoke extinction profiles to show that the largest extinction coefficients co-occur with high RH ($\sim 80\%$) at the top of the BBA layer. As discussed recently in Kar et al. (2018), this increase could be due to enhancement of the size of aged smoke during the transport over SAO.

A second important aspect of these results concerns the possible overestimates of the increase of extinction with RH as parameterized in the present version of ALADIN-Climate. As indicated for
1540 both cases, excellent agreement is generally observed in the extinction profiles even if some slight negative bias in RH remain. This can be clearly detected at 4500 m (09:00 UTC) or 4000 m (11:00

UTC). At 12:00 UTC and for altitudes between 1000 and 2000 m, RH simulated in SMK_SN is consistent with MERRA2 data, while the simulated extinction is overestimated.

1545 These original results, using for the first time coincident in-situ observations and nudged simulations (allowing the capture of the elevated humidity transported within smoke plume) of aerosol extinction within BBA plume, clearly indicate the significant impact of RH on BBA optical properties. This underlines the importance of including in models the fire processes related to the presence of humidity in the smoke plume over SAO. A second important aspect concerns the presence of possible errors in the actual parameterization used in ALADIN-Climate to calculate the evolution of BBA extinction with RH. In that sense, nudged simulations, associated with in-situ data obtained during ORACLES would certainly provide a unique opportunity to test and constrain the hydrophylic properties of BBA over SAO. Future work will extend significantly the number of cases studied to test the robustness of these first results.

5. Direct Radiative Forcing and impact of BBA

1555 5.1. DRF exerted at TOA

The monthly-mean DRF exerted at TOA (in the visible spectral range) is indicated in the Figure 13 in clear-sky (left) and all-sky (right) conditions. The ALADIN-Climate estimates do not include possible SST adjustments due to BBA radiative effects, even if this could be important over SAO (Sakaeda et al., 2011). Figure 13 indicates an important regional gradient in the sign of DRF over the domain in all-sky conditions, with a rather negative forcing over the continent (net cooling) and positive (net heating) over SAO. Over the continent, the mean DRF is found to be mostly negative (~-5/-15 W.m⁻²) over Angola, with local maxima up to -20 W.m⁻². An interesting result concerns the presence of significant positive forcings along the coast from Gabon to Namibia, with values of ~+10 to +20 W.m⁻². Such significant positive forcing at TOA are correlated with both the presence of Sc along the coast of Angola, Republic of Congo and Gabon (see Figure S6 in Supplement material) and the high surface albedo over Namibia (Figure 1).

On the contrary, over SAO, DRF exerted at TOA is found to be mainly positive in all-sky conditions in agreement with a large literature focused on this region (Meyer et al., 2013; Feng and Christopher, 2015; De Graaf et al., 2012, 2014; Zuidema et al., 2016). The impact of the presence of Sc on the sign of DRF at TOA is clearly shown when comparing the ALADIN-Climate simulations in clear-sky and all-sky conditions. The large cooling effect at TOA is replaced by a significant heating over a large part of SAO. However and when averaged over the same region (20°S–10°N and 10°W–20°E) as defined in Feng and Christopher (2015), an important underestimate is detected compared to satellite observations. Indeed, the instantaneous (at satellite time overpassing) monthly-averaged DRF is found to be about +6 W.m⁻² in ALADIN-Climate and ~+35 W.m⁻² in the

study of Feng and Christopher (2015). A better agreement is obtained with Oikawa et al. (2013), who reported an annual mean of $+3 \text{ W.m}^{-2}$ over Southern Africa using CALIPSO and GCM simulation. More recently, Gordon et al. (2018) indicate a regional DRF of $+11 \text{ W.m}^{-2}$ at TOA close to the one obtained in this study, but for five smoky days. We suspect the underestimate of LCF
1580 (Figure 2b) to be mostly responsible for this large difference with the Feng and Christopher (2015) estimates. **Interestingly**, comparisons with the climatological estimates based on MACC NRT data for the period 2010-2015 (Figure S7 of Supplement material) indicate important differences. Figure S7 indicates that the positive DRF simulated by ALADIN-Climate is absent in the MACC NRT data, except locally over the continent.

1585 **Finally, the SMK_SSA simulations indicate a significant changes in the monthly-mean (September 2016) DRF exerted at TOA, passing from a positive ($+4.2 \text{ W.m}^{-2}$) to negative (-0.54 W.m^{-2}) DRF (Figure 13 and Table 3) over the Box_O. This means that the positive DRF at TOA could be weaker at the end of BBA season (late october). Figure 13 indicates a more intense negative DRF at TOA over smoke sources due to more scattering BBA and over the box_S, the monthly-mean value
1590 (Table 3) is increasing from -3.9 W.m^{-2} (SMK) to -7.3 W.m^{-2} (SMK_SSA). In addition, a weaker positive DRF is observed at TOA along the Southern African coast and Gabon due to more scattering smoke.**

5.2. Impact on the continental surface energy budget and dynamics

The potential impact of BBA on the « continental climate » has been investigated by using the
1595 differences between the CTL and SMK simulations. Figure 14 shows the monthly-mean difference (September 2016) of the following variables; surface net SW radiations (upper left), 2-meter temperature (T2m, upper right), sensible heat fluxes (SHF, bottom left) and the PBL height (bottom right). The potential effect of BBA on the continental precipitation is not studied as little or no precipitation occurs south of approximately 8°S during the austral winter season.

1600 Smoke aerosols are responsible of an important dimming of about -30 to -50 W.m^{-2} (monthly mean) over the continent and -10 to -40 W.m^{-2} over SAO during September 2016, with the highest impact logically located over smoke sources. Such estimates are consistent with those reported by Sakaeda et al. (2011) or Tummon et al. (2010). This impact of BBA results in an important decrease in the T2m over Congo, Angola and Zambia, as well as certain regions of Southern Africa. The impact is
1605 approximately ~ -1 to $-3 \text{ }^{\circ}\text{C}$ over the continent, in good agreement with the values reported by Sakaeda et al. (2011). When averaged over box_S ($5-15^{\circ}\text{S} / 15-25^{\circ}\text{E}$), the impact of BBA on T2m is about -1.7°C during September 2016 (Figure 15a). The daily-mean impact of BBA remains constant during this period, except for the end of September when the effect is negligible. For the 26 to 31 September, we hypothesize that compensations should occur, the « dynamical » effect of

1610 BBA being more important than the « dimming » effect. As mentioned previously and contrary to Sakaeda et al. (2011), the impact of BBA on SST is not quantified as the ALADIN-Climate simulations have been performed with prescribed SST. Finally, it should be noted that the changes of the surface temperature per unit of AOD (averaged for all the period of simulation) is about $\sim -2.5^\circ$. This value is found to be higher than the one (-1.5° per unit AOD) reported by Zhang et al. (2016) for an extreme biomass burning event occurring over Central Canada during June 2015. The difference could be due to the absorbing properties of BBA, which are more pronounced in the present study compared to Zhang et al. (2016) with SSA of 0.94 (550 nm). This could favor higher dimming effect and related impact on the surface temperature over the Angola region.

In parallel with the changes in surface temperature, the sensible heat fluxes (SHF, Figure 14, bottom left) significantly decrease, meaning weaker fluxes, over almost the entire subcontinent, with maxima in the main biomass burning sources. The decrease is about -20 to -30 W.m^{-2} over the continent, with a mean value of -25 W.m^{-2} when averaged over the box_S (Figure 15b). The impact of smoke is important throughout the whole time period, with SHF changing from a (monthly-mean) value of 85 W.m^{-2} to 60 W.m^{-2} for the CTL and SMK runs, respectively. This is consistent with the findings of Sakaeda et al. (2011) or Tummon et al. (2010). Indeed, the latter report a decrease over almost the entire subcontinents, with a maximum (decrease of $\sim 50\%$) in the main smoke region. As a result of the significant decrease in T2m and SHF over much of the subcontinent, the PBL height (defined as the top of the PBL) also decreases in the SMK run. This decrease is significant over much of the subcontinent, in accordance with the results of Tummon et al. (2010), with regional maxima up to $\sim -400 \text{ m}$ (Figure 14, bottom right). The lowest changes are observed along the west coast between 10 and 15°S and small regions of increased PBL height occur over southern Namibia and Northern Angola consistent with increases in the surface temperature. When averaged over the continent (box_S), the decrease in the PBL height is also significant, changing from ~ 1200 to $\sim 1000 \text{ m}$ (monthly-averaged) for the CTL and SMK simulations (Figure 15c), respectively. The decrease is nearly constant during September 2016, except for 25 to 30 September (decrease), and not necessarily correlated with AOD. The difference in the PBL height can reach a maximum decrease of 300 m (Figure 15c). In parallel, the impact of BBA on the near-surface (10m) wind speed (not shown) indicates a general decrease (of about -0.5 m.s^{-1}) over most of the continent. Over the ocean, the impact is more complex with the presence of a contrast, characterized by an increase (decrease) of the surface wind around $0-10^\circ\text{W}/15-30^\circ\text{S}$ (latitudes higher than 15°S).

1640 Finally, the comparisons with the SMK_SSA simulations (not shown, Figure S8) indicate a decrease of the surface radiative forcing both over continent and ocean. As reported in Table 3, the monthly-

mean DRF at BOA is about -39 W.m^{-2} and -25 W.m^{-2} over Box_S for the SMK and SMK_SSA simulations, respectively (similar results are obtained over SAO). This is due to the decrease of SW radiations absorbed by smoke in the SMK_SSA simulation, increasing the SW radiations reaching the surface. This could be also due, to a lesser extent, to changes in the aerosol loading due to modifications of the dynamics and precipitations between the two simulations. This induces a less pronounced impact of BBA on the surface temperature and sensible heat fluxes in SMK_SSA. The increase of SW surface radiations, associated to lower absorption by BBA, decrease the impact on the PBL development (Figure S8). As mentioned previously, these results suggest that the impact of BBA on the surface fluxes and dynamics are certainly weaker at the end of the biomass burning season.

6. Conclusion

The transport, vertical structure, SW radiative heating, SW direct radiative forcing and climatic impact exerted by absorbing BBA in the SAO have been estimated for September 2016 using the ALADIN-Climate model in the context of the ORACLES and LASIC projects. The model is able to represent LWP and COD well, although with a large underestimate in LCF. The simulated BBA AOD is consistent over the continent (~ 0.7 at 550 nm) compared to MERRA2 or MODIS data and also locally against AERONET data. We have also used new recent retrievals of ACAOD (OMI or MODIS) to demonstrate the ability of the model to reproduce reasonable values of smoke concentrations above Sc during the transport over SAO.

The simulations indicate the transport of BBA over SAO mainly occurs between 2 and 4 km, consistent with aircraft lidar observations. There is some indication that the entrainment of BBA in the MBL could be underestimated by the model contrary to the recent literature (Zuidema et al., 2018). This possible bias could lead to underestimate the BBA indirect forcing in this ALADIN-Climate configuration. In parallel, the absorbing properties (SSA) of BBA are consistent over biomass-burning sources compared to AERONET but significantly higher when compared to Ascension Island (LASIC) surface observations. The significant difference could be due to the absence of internal mixing treatment in the model, a lack of representation of the long-range aging processes, and/or the absence of mixing of BBA in the MBL. In addition, the important SW absorption by BBA produces an additional SW heating of $\sim 1 \text{ }^\circ\text{K/day}$.

The ALADIN-Climate simulations reveal a significant regional gradient in the sign of the SW DRF at TOA (all-sky conditions and fixed SST conditions), with mostly negative (continent) and positive (SAO) forcing, mainly due to changes in the underlying albedo associated with highly absorbing BBA. Over the continent, an intense monthly-mean positive forcing ($+10/+15 \text{ W.m}^{-2}$) is simulated over the Gabon, part of the Congo and Angola, mainly due to the presence of low Sc. Over SAO, a

DRF of $+6 \text{ W.m}^{-2}$ (20°S – 10°N and 10°W – 20°E) is simulated at TOA during all the ORACLES-1 period.

1680 One of the main original results concerns the use of coincident in-situ observations and nudged simulations (allowing to capture the elevated humidity transported within smoke plume) of aerosol extinction within BBA plume. Results highlight the significant effect of enhanced moisture on BBA extinction that considerably reduces the negative bias (in the simulated extinction) in the nudged simulation (SMK_SN) with ORACLES-1 data, compared to the SMK (no nudging) run. A second
1685 important aspect concerns the possible errors in the actual parameterization used to estimate the changes in BBA extinction with RH in the model. Indeed, our results indicate a possible overestimate of the increase in smoke extinction due to RH when compared to ORACLES-1 observations. Nudged simulations, associated to in-situ observations, would certainly provide a unique data-set to test and constrain the hygroscopic properties of BBA over SAO. All of these
1690 points have possible implications for DRF considerations and future works will extend significantly the number of cases studied to test the robustness of the results.

For September 2016, the important negative surface dimming due to BBA (around -5 to -15 W.m^{-2}) over the subcontinent significantly modifies the surface energy budget over much of Southern Africa. Indeed, the decrease in the net surface SW radiations is compensated by a decrease in
1695 sensible heat fluxes (-25 W.m^{-2} , monthly mean) and surface land temperature ($-1.5 \text{ }^{\circ}\text{C}$) over Angola, Zambia and Congo notably. The association of the surface cooling and the lower tropospheric heating tends to decrease the continental PBL height over the continent by about $\sim 200 \text{ m}$.

Finally, the indirect radiative effect exerted by BBA remains to be investigated with the ALADIN-Climate model using ORACLES/CLARIFY/AEROCLO-SA data in a manner similar to that
1700 presented here for DRF considerations. Once evaluated for all forcings over this region, long-term simulations (ERA-INT period) will be done to assess the possible feedbacks of BBA on Sc properties and the regional radiative budget at a climatic scale.

1705

Author contribution

PN and MM designed the ALADIN-Climat configuration and MM performed the simulations. RR, DSM, PN developed the ALADIN-Climat model. AMS, MS, KM, HJ, OT and CH have participated
1710 to provide the different aerosol satellite products. PZ provided in-situ LASIC (Ascension Island) observations; SS and SC data from the SSFR instrument. SB and RF participated to provide the

HSRL-2 data. JR, RW, PS, PF and all co-authors have participated to the analysis of all observations and simulations. MM finalised the manuscript with contributions from all co-authors.

1715

1720

1725

1730

1735

1740

Acknowledgment

This work has been conducted in the frame of the ORACLES investigation under the National Aeronautics and Space Administration's Earth Venture program. The LASIC extinction and SSA values are available through doi:10.5439/1369240, obtained from the Atmospheric Radiation

1745

Measurement (ARM) User Facility, a U.S. Department of Energy (DOE) Office of Science user facility managed by the Office of Biological and Environmental Research. PZ acknowledges support from DOE ASR grant DE-SC0018272. AERONET data are available from 1750 <https://aeronet.gsfc.nasa.gov>. MODIS data are available from the NASA Level 1 and Atmospheres Data Center at <https://ladsweb.modaps.eosdis.nasa.gov/>. MODIS above-cloud data products are available from the authors on request. MISR data are available from the NASA Atmospheric Sciences Data Center at <https://eosweb.larc.nasa.gov/>. M. Mallet, P. Nabat and P. Formenti acknowledge the AErosols, Radiation and CLOUDs in southern Africa (Aeroclo-sA) project, 1755 supported by the French National Research Agency under grant agreement n° ANR-15-CE01-0014-01, the French national programme LEFE/INSU, the Programme national de Télédétection Spatiale (PNTS, <http://www.insu.cnrs.fr/pnts>), grants n° PNTS-2016-02 and PNTS-2016-14, the French National Agency for Space Studies (CNES), the Centre National de la Recherche Scientifique (CNRS), the South African National Research Foundation (NRF) under grant UID 105958, and the 1760 European Union's 7th Framework Programme (FP7/2014-2018) under EUFAR2 contract n°312609. We thank the CNRM Climate model development team.

1765

1770

1775

1780

1785

References

Adebisi, A. A., Zuidema, P., and S. J. Abel, S.J.: The convolution of dynamics and moisture with the presence of shortwave absorbing aerosols over the southeast Atlantic. *J. Climate*, 28,1997–2024, doi: 10.1175/JCLI-D-14-00 1790 352.1, 2015

- Adebiyi, A. and Zuidema, P.: The role of the southern African easterly jet in modifying the southeast Atlantic aerosol and cloud environments. *Q. J. R. Meteorol. Soc.*, 142 (April), p. 1574-1589 doi: [10.1002/qj.2765](https://doi.org/10.1002/qj.2765), 2016.
- 1795 Bellouin, N., J. Rae, A. Jones, C. Johnson, J. Haywood, and O. Boucher, O.: Aerosol forcing in the Climate Model Intercomparison Project (CMIP5) simulations by HadGEM2-ES and the role of ammonium nitrate, *J. Geophys. Res.*, 116,D20206, doi:10.1029/2011JD016074, 2011.
- 1800 Benedetti, A., Morcrette, J.-J., Boucher, O., Dethof, A., Engelen, R. J., Fisher, M., Flentjes, H., Huneeus, N., Jones, L., Kaiser, J. W., Kinne, S., Mangold, A., Razinger, M., Simmons, A. J., Suttie, M., and the GEMS-AER team: Aerosol analysis and forecast in the ECMWF Integrated Forecast System: 2. Data assimilation, *J. Geophys. Res.*, 114, D13205, <https://doi.org/10.1029/2008JD011115>, 2009.
- 1805 Benas, N., Finkensieper, S., Stengel, M., van Zadelhoff, G.-J., Hanschmann, T., Hollmann, R., and Meirink, J. F.: The MSG-SEVIRI-based cloud property data record CLAAS-2, *Earth Syst. Sci. Data*, 9, 415-434, <https://doi.org/10.5194/essd-9-415-2017>, 2017.
- 1810 Burton, S. P., Hair, J. W., Kahnert, M., Ferrare, R. A., Hostetler, C. A., Cook, A. L., Harper, D. B., Berkoff, T. A., Seaman, S. T., Collins, J. E., Fenn, M. A., and Rogers, R. R.: Observations of the spectral dependence of linear particle depolarization ratio of aerosols using NASA Langley airborne High Spectral Resolution Lidar, *Atmos. Chem. Phys.*, 15, 13453-13473, 10.5194/acp-15-13453-2015, 2015.
- 1815 Burton, S. P., Hostetler, C., Cook, A., Hair, J., Seaman, S. T., Scola, S. J., Harper, D., Smith, J. A., Fenn, M. A., Ferrare, R., Saide, P. E., Chemyakin, E., and Müller, D.: Calibration of a high spectral resolution lidar using a Michelson interferometer, with data examples from ORACLES, *Appl Opt*, 2018, in press.
- 1820 Chand, D., R. Wood, T. L. Anderson, S. K. Satheesh, and R. J. Charlson. "Satellite-Derived Direct Radiative Effect of Aerosols Dependent on Cloud Cover." *Nature Geoscience* 2, no. 3 (March 2009): 181–84. <https://doi.org/10.1038/ngeo437>, 2009.
- Cochrane, S., K., S. Schmidt, H. Chen, P. Pilewskie, S. Kittelman, W. Gore, J. Redemann, S. LeBlanc, K. Pistone, S. Platnick, K. Meyer, R. Ferrare, S. Burton, C. Hostetler, and Dobracki, A.: Aircraft-Derived Above-Cloud Aerosol Radiative Effects Based on ORACLES 2016 and ORACLES 2017 Experiments, in preparation in ACP, 2018.
- 1825 Cubison, M. J., Ortega, A. M., Hayes, P. L., Farmer, D. K., Day, D., Lechner, M. J., Brune, W. H., Apel, E., Diskin, G. S., Fisher, J. A., Fuelberg, H. E., Hecobian, A., Knapp, D. J., Mikoviny, T., Riemer, D., Sachse, G. W., Sessions, W., Weber, R. J., Weinheimer, A. J., Wisthaler, A., and Jimenez, J. L.: Effects of aging on organic aerosol from open biomass burning smoke in aircraft and laboratory studies, *Atmos. Chem. Phys.*, 11, 12049-12064, <https://doi.org/10.5194/acp-11-12049-2011>, 2011.
- 1830 Das, S., H. Harshvardhan, H. Bian, M. Chin, G. Curci, A. P. Protonotariou, T. Mielonen, K. Zhang, H. Wang, and Liu, X.: Biomass burning aerosol transport and vertical distribution over the South African-Atlantic region, *J. Geophys. Res. Atmos.*, 122, 6391–6415, doi:10.1002/2016JD026421, 2017.
- 1835 De Graaf, M., L. G. Tilstra, P. Wang, and Stammes, P.: Retrieval of the aerosol direct radiative effect over clouds from spaceborne spectrometry, *J. Geophys. Res.*, 117, D07207, doi:10.1029/2011JD017160, 2012.
- 1840 De Graaf, M., N. Bellouin, L. G. Tilstra, J. Haywood, and Stammes, P.: Aerosol direct radiative effect of smoke over clouds over the southeast Atlantic Ocean from 2006 to 2009, *Geophys. Res. Lett.*, 41, 7723–7730, doi:10.1002/2014GL061103, 2014.
- ~~Dentener, F., Kinne, S., Bond, T., Boucher, O., Cofala, J., Generoso, S., et al.: Emissions of primary aerosol and precursor gases in the years 2000 and 1750 prescribed data sets for AeroCom. *Atmospheric Chemistry and Physics*, 6, 4321–4344. <https://doi.org/10.5194/acp-6-4321-2006>, 2006.~~
- 1845 Diamond, M. S., Dobracki, A., Freitag, S., Small Griswold, J. D., Heikkila, A., Howell, S. G., Kacarab, M. E., Podolske, J. R., Saide, P. E., and Wood, R.: Time-dependent entrainment of smoke presents an observational challenge for assessing aerosol–cloud interactions over the southeast Atlantic Ocean, *Atmos. Chem. Phys. Discuss.*, <https://doi.org/10.5194/acp-2018-461>, in review, 2018.
- 1850

- Dubovik, O., and King, M.D.: A flexible inversion algorithm for retrieval of aerosol optical properties from Sun and sky radiance measurements, *J. Geophys. Res.*, 105(D16), 20673–20696, doi: 10.1029/2000JD900282, 2000.
- 1855 Dubovik, O., A. Smirnov, B. N. Holben, M. D. King, Y. J. Kaufman, T. F. Eck, and Slutsker I.: Accuracy assessments of aerosol optical properties retrieved from Aerosol Robotic Network (AERONET) Sun and sky radiance measurements, *J. Geophys. Res.*, 105(D8), 9791–9806, doi: 10.1029/2000JD900040, 2000.
- 1860 Eck, T. F., et al.: A seasonal trend of single scattering albedo in southern African biomass-burning particles: Implications for satellite products and estimates of emissions for the world's largest biomass-burning source, *J. Geophys. Res. Atmos.*, 118, 6414–6432, doi:10.1002/jgrd.50500, 2013.
- Fierce, L., T.C. Bond, S.E. Bauer, F. Mena, and Riemer, N.: Black carbon absorption at the global scale is affected by particle-scale diversity in composition. *Nature Commun.*, 7, 12361, doi:10.1038/ncomms12361, 2016.
- 1865 Feng, N. and Christopher, S.A.: Measurement-based estimates of direct radiative effects of absorbing aerosols above clouds, *J. Geophys. Res. Atmos.*, vol. 120, no. 14, pp. 6908–6921, 2015.
- 1870 Fierce, L. et al., Black carbon absorption at the global scale is affected by particle-scale diversity in composition. *Nat. Commun.* 7:12361 doi: 10.1038/ ncomms12361, 2016.
- Gelaro, R., McCarty, W., Suárez, M. J., Todling, R., Molod, A., Takacs, L., Randles, C. A., Darmenov, A., Bosilovich, M. G., and Reichle, R.: The modern-era retrospective analysis for research and applications, version 2 (MERRA-2), *J Climate*, 30, 5419–5454, 10.1175/JCLI-D-16-0758.1, 2017.
- 1875 Gordon, H., Field, P. R., Abel, S. J., Johnson, B. T., Dalvi, M., Grosvenor, D. P., Hill, A. A., Miltenberger, A. K., Yoshioka, M., and Carslaw, K. S.: Large simulated radiative effects of smoke in the south-east Atlantic, *Atmos. Chem. Phys. Discuss.*, <https://doi.org/10.5194/acp-2018-305>, in review, 2018.
- 1880 Hair, J. W., Hostetler, C. A., Cook, A. L., Harper, D. B., Ferrare, R. A., Mack, T. L., Welch, W., Izquierdo, L. R., and Hovis, F. E.: Airborne High Spectral Resolution Lidar for profiling aerosol optical properties, *Appl Optics*, 47, 6734–6752, 10.1364/AO.47.006734, 2008.
- 1885 Haywood, J., S. R. Osborne, P. N. Francis, A. Keil, P. Formenti, M. O. Andreae, and P. H. Kaye: The mean physical and optical properties of regional haze dominated by biomass burning aerosol measured from the C-130 aircraft during SAFARI 2000, *J. Geophys. Res.*, 108, 8473, doi:10.1029/2002JD002226, 2003.
- Hodnebrog, O., Myhre, G., Forster, P. M., Sillmann, J., and Samset, B. H.: Local biomass burning is a dominant cause of the observed precipitation reduction in southern Africa, *Nat. Commun.*, 7, 11236, 2016.
- 1890 Jethva, H., Torres, O., and Ahn, C.: A 12-Year Long Global Record of Optical Depth of Absorbing Aerosols above the Clouds Derived from OMI/OMACA Algorithm, [11, 5837-5864, https://doi.org/10.5194/amt-11-5837-2018](https://doi.org/10.5194/amt-11-5837-2018), 2018.
- 1895 Johnson, B. T., Shine, K. P., & Forster, P. M.: The semi-direct aerosol effect: Impact of absorbing aerosols on marine stratocumulus. *Quarterly Journal of the Royal Meteorological Society*, 130, 1407–1422, 2004.
- 1900 Johnson, B. T., Haywood, J. M., Langridge, J. M., Darbyshire, E., Morgan, W. T., Szpek, K., Brooke, J. K., Marengo, F., Coe, H., Artaxo, P., Longo, K. M., Mulcahy, J. P., Mann, G. W., Dalvi, M., and Bellouin, N.: Evaluation of biomass burning aerosols in the HadGEM3 climate model with observations from the SAMBBA field campaign, *Atmos. Chem. Phys.*, 16, 14657–14685, <https://doi.org/10.5194/acp-16-14657-2016>, 2016.
- 1905 Kahn, R. A., and Gaitley, B.J.: An analysis of global aerosol type as retrieved by MISR, *J. Geophys. Res. Atmos.*, 120, 4248–4281, doi:10.1002/2015JD023322, 2015.
- 1905 Kar, J., Vaughan, M., Tackett, J., Liu, Z., Omar, A., Rodier, S., Trepte, C., and Lucker, P.: Swelling of transported smoke from savanna fires over the Southeast Atlantic Ocean, *Rem. Sen. Env.*, 211, 105–111, <https://doi.org/10.1016/j.rse.2018.03.043>, 2018.
- 1910 Labonne, M., Breon, F.-M., Chevallier, F.: Injection height of biomass burning aerosols as seen from a spaceborne lidar. *Geophysical Research Letters*, 34, L11806. <https://doi.org/10.1029/2007GL029311>, 2007.

- Mallet, M., Solmon, F., Roblou, L., Peers, F., Turquety, S., Waquet, F., Jethva, H, Torres, O.: Simulation of Optical Properties and Direct and Indirect Radiative Effects of Smoke Aerosols Over Marine Stratocumulus Clouds During Summer 2008 in California With the Regional Climate Model RegCM, *Journal of Geophys. Res.-Atmosphere*, 122, 10288-10313, 2017.
- 1915 **Marticorena, B. and Bergametti, G.: Modeling the atmosphere dustcycle: 1. Design of a soil-derived dust emission scheme, *J. Geo-phys. Res.*, 100, 16415–16430, 1995.**
- Martin, G. M., Johnson, D. W., and Spice, A.: The measurement and parameterization of effective radius of droplets in warm stratiform clouds, *J. Atmos. Sci.*, 51, 1823–1842, 1994.
- 1920
- Masson, V., Le Moigne, P., Martin, E., Faroux, S., Alias, A., Alkama, R., Belamari, S., Barbu, A., Boone, A., Bouysse, F., Brousseau, P., Brun, E., Calvet, J.-C., Carrer, D., Decharme, B., Delire, C., Donier, S., Essaouini, K., Gibelin, A.-L., Giordani, H., Habets, F., Jidane, M., Kerdraon, G., Kourzeneva, E., Lafaysse, M., Lafont, S., Lebeaupin Brossier, C., Lemonsu, A., Mahfouf, J.-F., Marguinaud, P., Mokhtari, M., Morin, S., Pigeon, G., Salgado, R., Seity, Y., Taillefer, F., Tanguy, G., Tulet, P., Vincendon, B., Vionnet, V., and Voldoire, A.: The SURFEXv7.2 land and ocean surface platform for coupled or offline simulation of earth surface variables and fluxes, *Geosci. Model Dev.*, 6, 929-960, <https://doi.org/10.5194/gmd-6-929-2013>, 2013.
- 1925
- Mayer, B. and Kylling, A.: Technical note: The libRadtran software package for radiative transfer calculations - description and examples of use, *Atmos. Chem. Phys.*, 5, 1855-1877, <https://doi.org/10.5194/acp-5-1855-2005>, 2005.
- 1930
- Meyer, K., S. Platnick, L. Oreopoulos, and Lee D.: Estimating the direct radiative effect of absorbing aerosols overlying marine boundary layer clouds in the southeast Atlantic using MODIS and CALIOP, *J. Geophys. Res. Atmos.*, 118, 4801–4815, doi:10.1002/jgrd.50449, 2013.
- 1935
- Meyer K., Platnick S., and Zhang Z.: Simultaneously inferring above-cloud absorbing aerosol optical thickness and underlying liquid phase cloud optical and microphysical properties using MODIS, *J Geophys Res. Atmos.*, 119, 5104–5114, doi:10.1002/2013JD021053, 2015.
- 1940
- Mlawer, E.J., Taubman, S.J., Brown, P.D., Iacono, M.J. and Clough, S.A. : Radiative transfer for inhomogeneous atmospheres: RRTM, a validated correlated-k model for the longwave, *Journal of Geophysical Research* 102: doi: 10.1029/97JD00237. Issn: 0148-0227, 1997.
- 1945
- Morcrette JJ : Description of the radiation scheme in the ecmwf model. Tech. rep, ECMWF, 1989.
- Michou, M., Nabat, P., and Saint-Martin, D.: Development and basic evaluation of a prognostic aerosol scheme (v1) in the CNRM Climate Model CNRM-CM6, *Geosci. Model Dev.*, 8, 501-531, [DOI:10.5194/gmd-8-501-2015](https://doi.org/10.5194/gmd-8-501-2015), 2015.
- 1950
- Ogren, J.: Comment on “Calibration and Intercomparison of Filter-Based Measurements of Visible Light Absorption by Aerosols.”. *Aerosol Sci. Technol.*, 44: 589–591, 2010.
- Oikawa, E., T. Nakajima, T. Inoue, and Winker D.: A study of the shortwave direct aerosol forcing using ESSP/CALIPSO observation and GCM simulation, *J. Geophys. Res. Atmos.*, 118, 3687–3708, doi:10.1002/jgrd.50227, 2013.
- 1955
- Nabat, P., Somot, S., Mallet, M., Sevault, F., Chiacchio, M., and Wild, M.: Direct and semi-direct aerosol radiative effect on the Mediterranean climate variability using a coupled regional climate system model, *Clim. Dynam.*, 44, 1127–1155, doi:10.1007/s00382-014-2205-6, 2015a.
- 1960
- Nabat, P., Somot, S., Mallet, M., Michou, M., Sevault, F., Driouech, F., Meloni, D., di Sarra, A., Di Biagio, C., Formenti, P., Sicard, M., Léon, J.-F., and Bouin, M.-N.: Dust aerosol radiative effects during summer 2012 simulated with a coupled regional aerosol– atmosphere–ocean model over the Mediterranean, *Atmos. Chem. Phys.*, 15, 3303–3326, doi:10.5194/acp-15-3303-2015, 2015b.
- 1965
- Nakajima, T., and King, M.D.: Determination of the Optical Thickness and Effective Particle Radius of Clouds from Reflected Solar Radiation Measurements. Part 1: Theory. *J. Atmos. Sci.*, 47, 1878-1893, 1990.
- Nam, C., Bony, S., Dufresne, J.-L., and Chepfer, H.: The ‘too few, too bright’ tropical low-cloud problem in CMIP5 models. *Geophys. Res. Letters*, 39 (21), 2012.
- 1970

- 1975 Petrenko, M., Kahn, R., Chin, M., and Limbacher, J.: Refined use of satellite aerosol optical depth snapshots to constrain biomass burning emissions in the GOCART model. *Journal of Geophysical Research: Atmospheres*, 122, 10,983–11,004. <https://doi.org/10.1002/2017JD026693>, 2017.
- Radu, R., M. Déqué, and S. Somot, S.: Spectral nudging in a spectral regional climate model. *Tellus*, 60A, 898–910, doi:10.1111/j.1600-0870.2008.00341.x, 2008.
- 1980 Reid, J. S., Eck, T. F., Christopher, S. A., Koppmann, R., Dubovik, O., Eleuterio, D. P., Holben, B. N., Reid, E. A., and Zhang, J.: A review of biomass burning emissions part III: intensive optical properties of biomass burning particles, *Atmos. Chem. Phys.*, 5, 827-849, <https://doi.org/10.5194/acp-5-827-2005>, 2005.
- 1985 Roebeling, R.A., A.J. Feijt and Stammes, P.: Cloud property retrievals for climate monitoring: implications of differences between SEVIRI on METEOSAT-8 and AVHRR on NOAA-17, *J. Geophys. Res.*, 111, D20210, doi:10.1029/2005JD006990, 2006.
- Sakaeda, N., R. Wood, and Rasch, P.J.: Direct and semidirect aerosol effects of southern African biomass burning aerosol, *J. Geophys. Res.*, 116, D12205, doi:10.1029/2010JD015540, 2011.
- 1990 Sayer, A. M., L. A. Munchak, N. C. Hsu, R. C. Levy, C. Bettenhausen, and Jeong, M.-J.: MODIS Collection 6 aerosol products: Comparison between Aqua's e-Deep Blue, Dark Target, and “merged” data sets, and usage recommendations, *J. Geophys. Res. Atmos.*, 119, 13,965–13,989, doi: 10.1002/2014JD022453, 2014.
- 1995 Sayer A. M., N. C. Hsu, C. Bettenhausen, J. Lee, J. Redemann, B. Schmid, and Shinozuka, Y.: Extending “Deep Blue” aerosol retrieval coverage to cases of absorbing aerosols above clouds: Sensitivity analysis and first case studies, *J. Geophys. Res. Atmos.*, 121, 4830–4854, doi: 10.1002/2015JD024729, 2016.
- 2000 Sayer, A. M., Hsu, N. C., Lee, J., Kim, W. V., Burton, S., Fenn, M. A., Ferrare, R. A., Kacenelenbogen, M., LeBlanc, S., Pistone, K., Redemann, J., Segal-Rozenhaimer, M., Shinozuka, Y., and Tsay, S.-C.: Two decades observing smoke above clouds in the south-eastern Atlantic Ocean: Deep Blue algorithm updates and validation with ORACLES field campaign data, *Atmos. Meas. Tech. Discuss.*, <https://doi.org/10.5194/amt-2019-58>, in review, 2019.
- 2005 Schulz, M., de Leeuw, G., and Balkanski, Y.: Sea-salt aerosol source functions and emissions, in: *Emission of Atmospheric Trace Compounds*, edited by: Granier, C., Artaxo, P., and Reeves, C. E., Kluwer Acad., Norwell, Mass., Springer Netherlands, 333-359, 2004.
- 2010 Seethala, C., Meirink, J. F., Horváth, Á., Bennartz, R., and Roebeling, R.: Evaluating the diurnal cycle of South Atlantic stratocumulus clouds as observed by MSG SEVIRI, *Atmos. Chem. Phys.*, 18, 13283-13304, <https://doi.org/10.5194/acp-18-13283-2018>, 2018.
- 2015 Shinozuka, Y., P. E. Saide, S. P. Burton, P. Zuidema, G. A. Ferrada, M. Mallet, Y. Zhang, R. Leung, L. Pfister, J.-M. Ryoo, S. G. Howell, S. Freitag, A. Dobracki, J. R. Podolske, S. LeBlanc, R. Ferrare, D. Henze, D. Noone, M. Kacarab, A. Nenes, E. J. Stith, J. R. Bennett, G. R. Carmichael, S. J. Doherty, R. Wood, and Redemann, J.: Global and regional modeling of absorbing aerosols in the southeast Atlantic during ORACLES 2016: comparisons to new observations, in preparation in ACPD, 2019.
- 2020 Shipley, S. T., Tracy, D. H., Eloranta, E. W., Trauger, J. T., Sroga, J. T., Roesler, F. L., and Weinman, J. A.: High Spectral Resolution Lidar to Measure Optical-Scattering Properties of Atmospheric Aerosols .I. Theory and Instrumentation, *Appl Optics*, 22, 3716-3724, 10.1364/AO.22.003716, 1983.
- Slingo, A. and Schrecker, H.M. : On the shortwave radiative properties of stratiform water clouds. *Q. J. R. Meteorol. Soc.*,108: 407-426, 1982.
- 2025 Stephens, G. : Radiation profiles in extended water clouds, II : Parametrization schemes, *J. Atmos. Sci.*, 35, 2123-2132, 1978.
- Stengel, M., Kniffka, A., Meirink, J. F., Lockhoff, M., Tan, J., and Hollmann, R.: CLAAS: the CM SAF cloud property data set using SEVIRI, *Atmos. Chem. Phys.*, 14, 4297-4311, <https://doi.org/10.5194/acp-14-4297-2014>, 2014.

- 2030 Stier, P., Schutgens, N. A. J., Bellouin, N., Bian, H., Boucher, O., Chin, M., Ghan, S., Huneeus, N., Kinne, S., Lin, G., Ma, X., Myhre, G., Penner, J. E., Randles, C. A., Samset, B., Schulz, M., Takemura, T., Yu, F., Yu, H., and Zhou, C.: Host model uncertainties in aerosol radiative forcing estimates: results from the AeroCom Prescribed intercomparison study, *Atmos. Chem. Phys.*, 13, 3245-3270, <https://doi.org/10.5194/acp-13-3245-2013>, 2013.
- 2035 Sun, Q., Wang, Z., Li, Z., Erb, A., & Schaaf, C. B.: Evaluation of the Global MODIS 30 Arc-Second Spatially and Temporally Complete Snow-Free Land Surface Albedo and Reflectance Anisotropy Dataset. *International Journal of Applied Earth Observation and Geoinformation*, 58, 36–49, 2017.
- 2040 Tummon, F., F. Solmon, C. Lioussé, and Tadross, M. : Simulation of the direct and semidirect aerosol effects on the southern Africa regional climate during the biomass burning season, *J. Geophys. Res.*, 115, D19206, doi:10.1029/2009JD013738, 2010.
- 2045 Vakkari, V., Beukes, J.P., Dal Maso, M., Aurela, M., Josipovic, M., and Van Zyl, P.G.: Major secondary aerosol formation in southern African open biomass burning plumes, *Nature Geoscience*, 1-4, 2018.
- van Marle, M. J. E., Kloster, S., Magi, B. I., Marlon, J. R., Daniau, A.-L., Field, R. D., Arneth, A., Forrest, M., Hantson, S., Kehrwald, N. M., Knorr, W., Lasslop, G., Li, F., Mangeon, S., Yue, C., Kaiser, J. W., and van der Werf, G. R.: Historic global biomass burning emissions for CMIP6 (BB4CMIP) based on merging satellite observations with proxies and fire models (1750–2015), *Geosci. Model Dev.*, 10, 3329-3357, <https://doi.org/10.5194/gmd-10-3329-2017>, 2017.
- 2050 Virkkula, A.: Correction of the Calibration of the 3-wavelength Particle Soot Absorption Photometer (3 λ PSAP), *Aerosol Science and Technology*, 44:8, 706-712, DOI: [10.1080/02786826.2010.482110](https://doi.org/10.1080/02786826.2010.482110), 2010.
- 2055 Xu, H., Guo, J. P., Ceamanos, X., Roujean, J. L., Min, M., Carrer, D.: On the influence of the diurnal variations of aerosol content to estimate direct aerosol radiative forcing using MODIS data. *Atmospheric Environment*, 141, 186–196. <https://doi.org/10.1016/j.atmosenv.2016.06.067>, 2016.
- 2060 Wilcox, E. M.: Stratocumulus cloud thickening beneath layers of absorbing smoke aerosol, *Atmos. Chem. Phys.*, 10, 11769-11777, <https://doi.org/10.5194/acp-10-11769-2010>, 2010.
- Zhang, J., Reid, J. S., Christensen, M., and Benedetti, A.: An evaluation of the impact of aerosol particles on weather forecasts from a biomass burning aerosol event over the Midwestern United States: observational-based analysis of surface temperature, *Atmos. Chem. Phys.*, 16, 6475-6494, <https://doi.org/10.5194/acp-16-6475-2016>, 2016.
- 2065 Zuidema P, et al.: Smoke and clouds above the southeast Atlantic: Upcoming field campaigns probe absorbing aerosols impact on climate. *Bull Am Meteorol Soc* 97:1131 – 1135, 2016.
- 2070 Zuidema, P., A. Sedlacek, C. Flynn, S. Springston, R. Delgado, J. Zhang, A. Aiken and Muradyan, P. The Ascension Island boundary layer in the remote southeast Atlantic is often smoky. *Geophys. Res. Lett.*, **45**, pp. 4456-4465 doi:[10.1002/2017GL076926](https://doi.org/10.1002/2017GL076926), 2018.

2075

2080

Aerosol Species	r_0	σ	Density	n / k	MEE	SSA	ASY
<i>Fresh smoke</i>	0.10	1.30	1.350	1.50 / 0.03	4.05	0.84	0.51
<i>Aged smoke</i>	0.12	1.30	1.350	1.50 / 0.03	5.05	0.90	0.58

Note. Here r_0 and σ are the median radius (in μm) and geometric standard deviation of the lognormal distribution. Mass density is reported in $\text{g}\cdot\text{cm}^{-3}$, m is the complex refractive index, and MEE and SSA the mass extinction efficiency (m^2g^{-1}) and single scattering albedo in dry state and reported at 550 nm.

2085 **Table 1.** Parameters describing aerosol components used in the ALADIN-Climate model for the
two smoke tracers and the resulting optical properties.

2090

2095

2100

2105

2110

	Aerosols	Clouds	Spatial / Temporal Resolutions	Available Period
MOD06ACAERO	ACAOD	#	0.1 × 0.1 ° / daily	June-Oct. 2000(T)/03(A) - 2019
MODIS DB	ACAOD	#	0.5 × 0.5 °/daily	2000(T)/02(A) - 2017

MODIS DT/DB	AOD	LWP, COD	1 × 1 ° / daily	2000 - 2019
OMI	ACAOD	#	0.5 × 0.5 ° / daily	2004 - 2019
MISR	AOD	#	0.5 × 0.5 ° / monthly	2000 - 2017
SEVIRI	#	LWP, COD	0.5 × 0.5 ° / daily	2004 - 2015
ERA-Interim	#	LWP, LCF	0.7 × 0.7 ° / daily	1979 - 2018
MERRA2	AOD by species	#	0.5 × 0.625 ° / hourly	1980 - 2018
CAMS	AOD by species	#	0.5 × 0.625 ° / hourly	2008 - 2015
MACC	DRF TOA (all-sky)	#	1.125 × 1.125 ° / daily	2003 - 2011

2115

Table 2. Satellite (T:Terra, A:Aqua) and reanalysis data used in this study to analyse aerosols and Sc clouds microphysical/optical properties.

2120

2125

2130

2135

	DRF_BOA		DRF_TOA		SW Heating (3 km)	
	Box_S	Box_O	Box_S	Box_O	Box_S	Box_O
ALD_SMK	-38.93	-15.73	-3.92	+4.22	1.15	0.75
ALD_SMK_SSA	-24.81	-8.17	-7.37	-0.54	0.58	0.30

2140 **Table 3.** Monthly mean (September 2016) all-sky direct radiative forcing at TOA and BOA ($\text{W}\cdot\text{m}^{-2}$) and SW heating rate at 3 km ($^{\circ}\text{K}/\text{day}$) for the two boxes (Box_S and Box_O), obtained from the SMK and SMK_SSA simulations.

2145

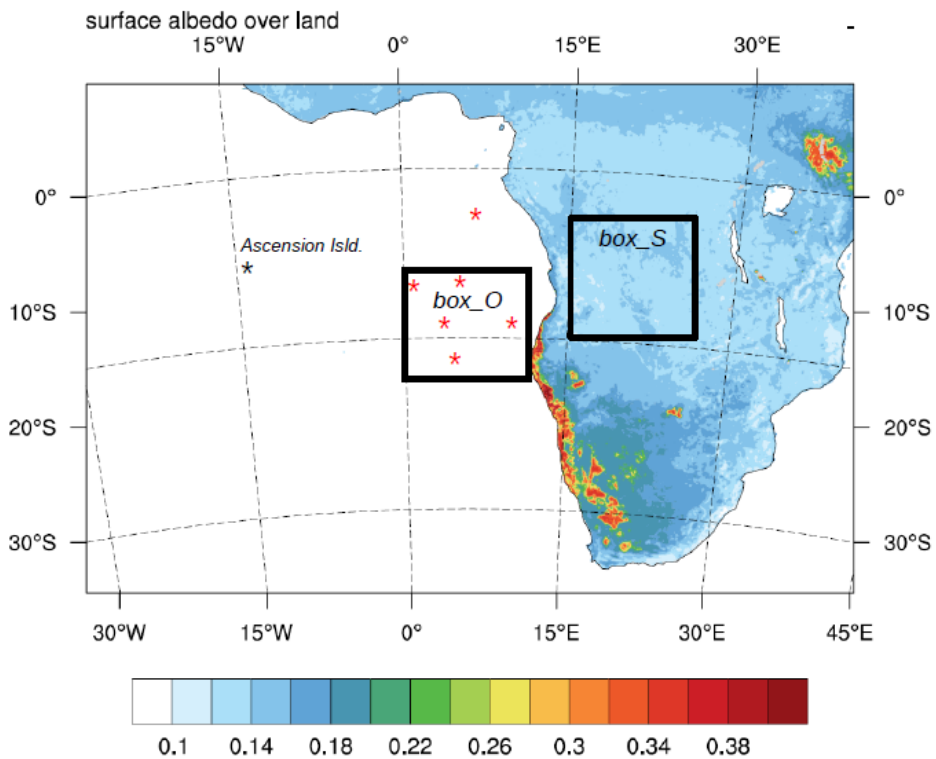
2150

2155

2160

2165

2170

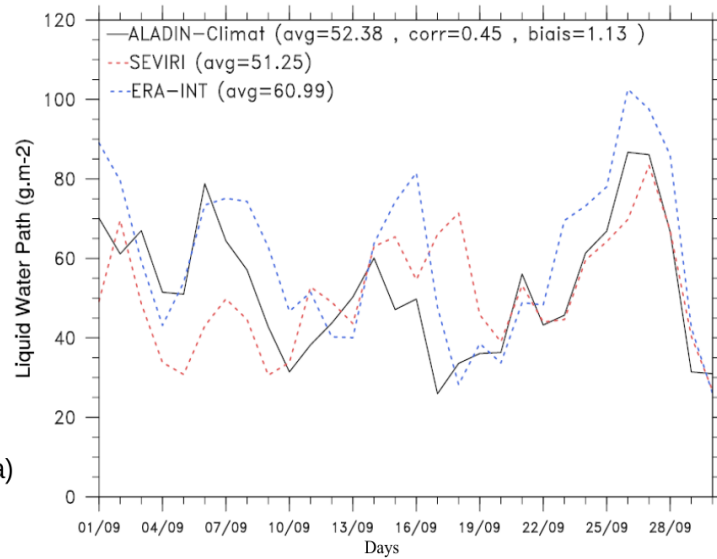


2175

2180

2185

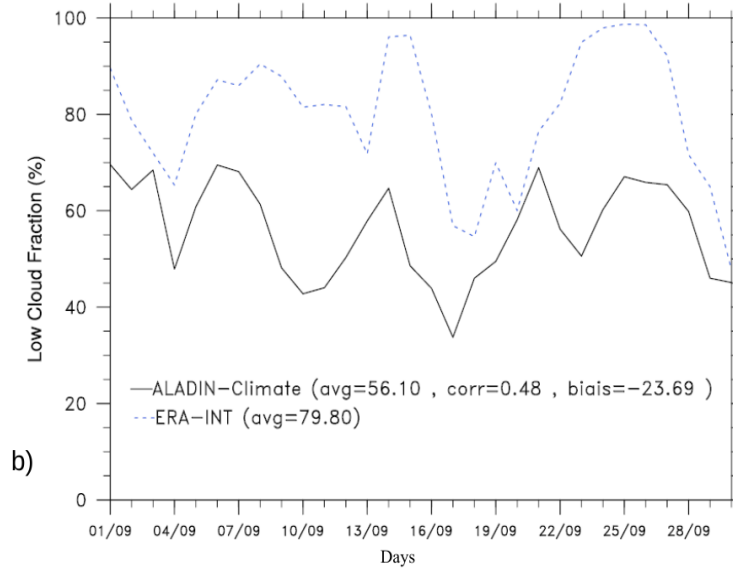
2190 **Figure 1.** Domain
ALADIN-Climate
(here, the surface
represented). The
(box_O and box_S) a)
2195 Island are indicated.
the localisation of
studied in the Part



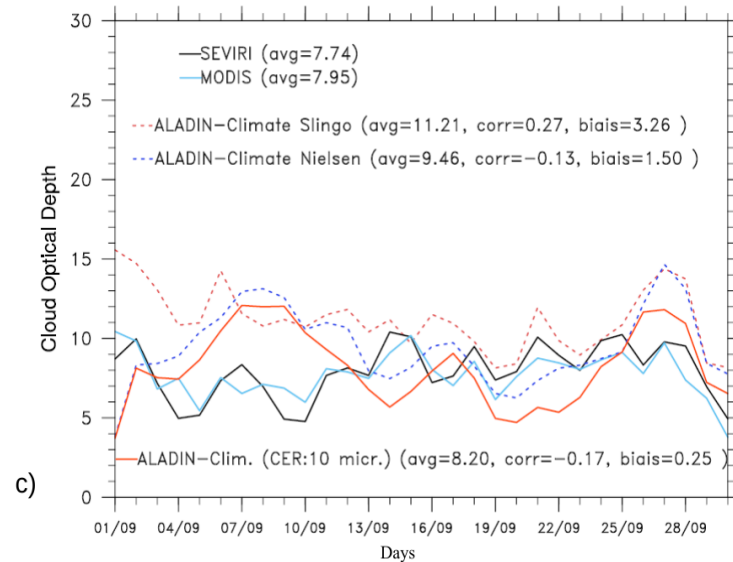
defined for the
model simulations
albedo is
two different boxes
and the Ascension
Red stars represent
different profiles
4.2.3.2.

2200

2205



2210



2215

2220

2225

2230

2235

2240

2245 **Figure 2.** Daily-mean Sc properties (LWP, LCF and COD) simulated by ALADIN-Climate and from ERA-INT and SEVERI data. Values have been averaged over the box_O.

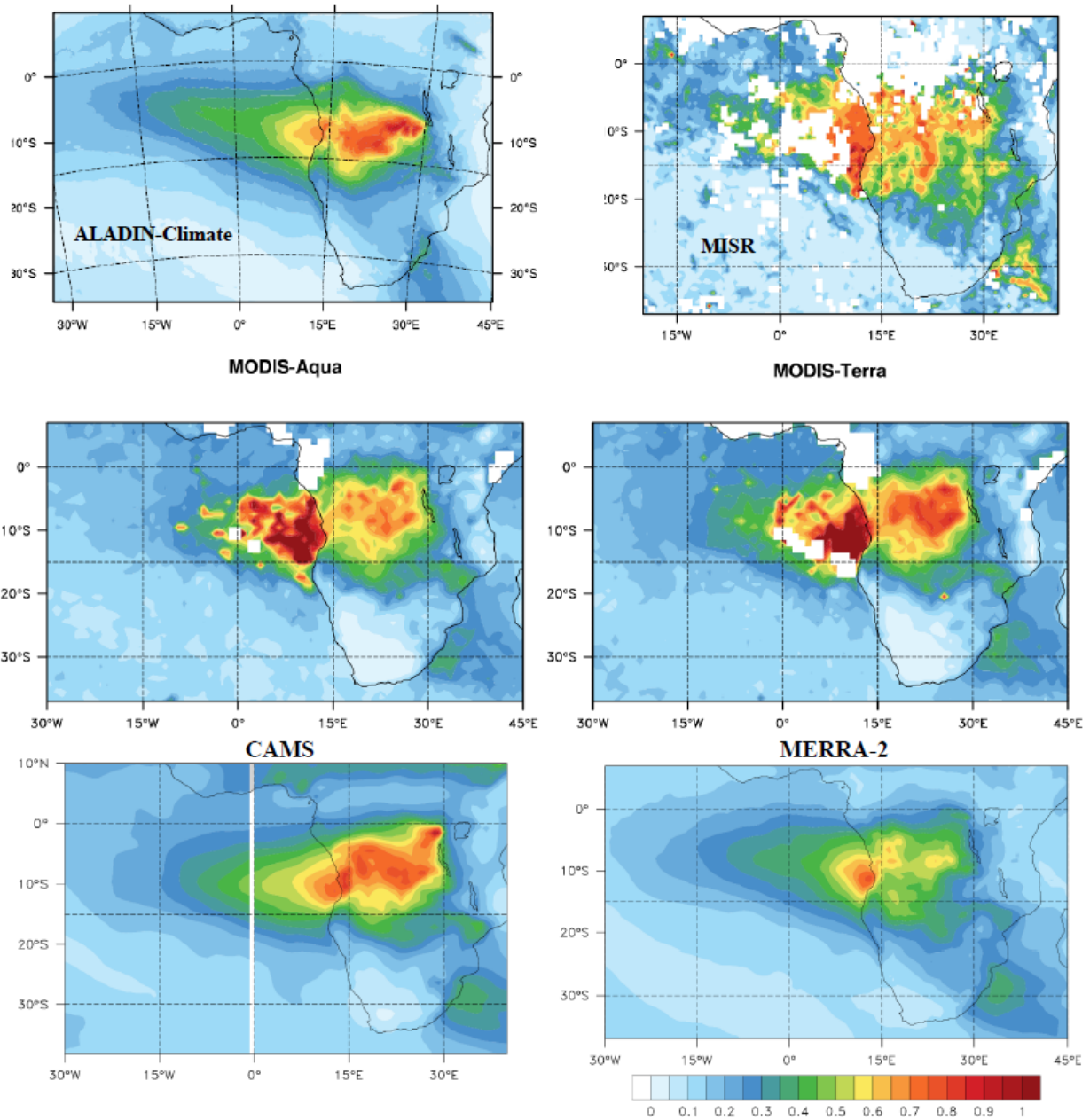


Figure 3. Total monthly-averaged Total AOD (at 550 nm) for september 2016 simulated by ALADIN-Climate (all times used), CAMS, MERRA2 and derived from the MODIS Terra, Aqua 2250 (combined DB/DT products) and MISR sensors.

2255

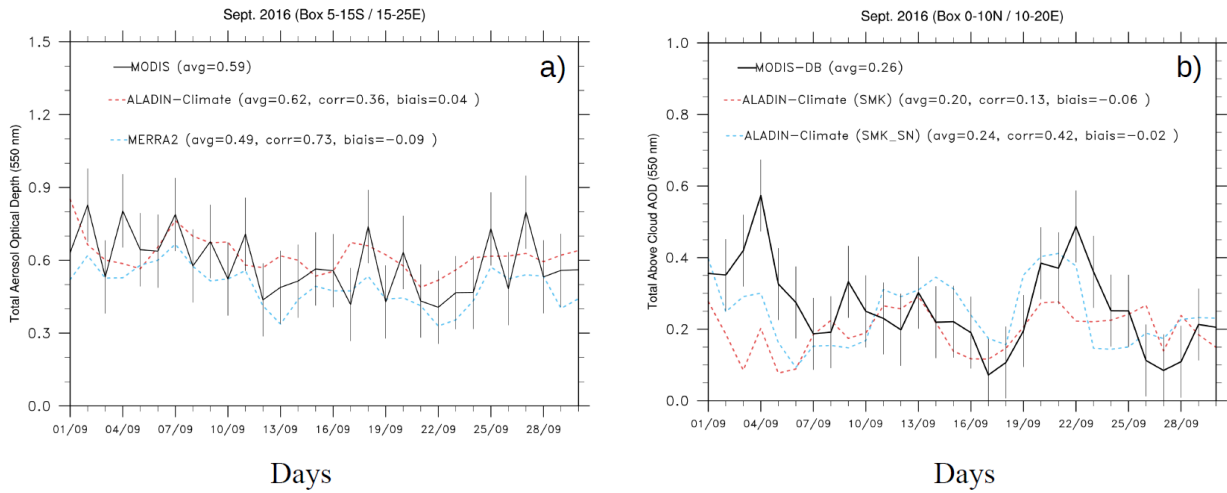
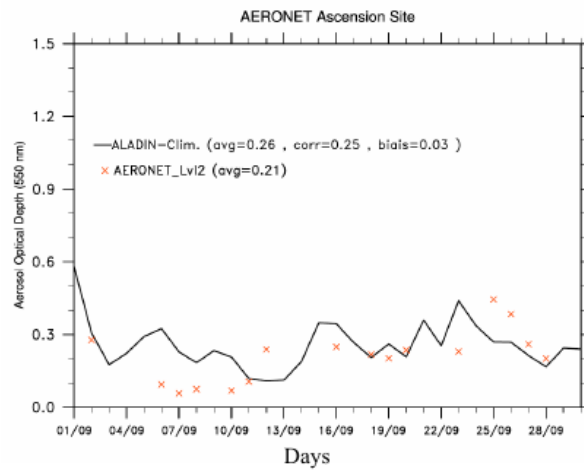
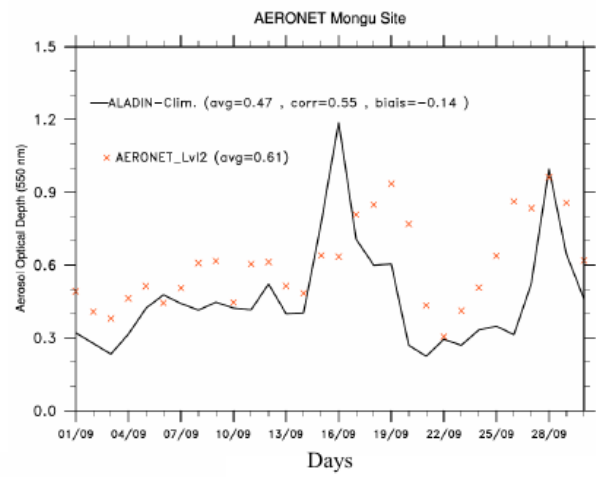
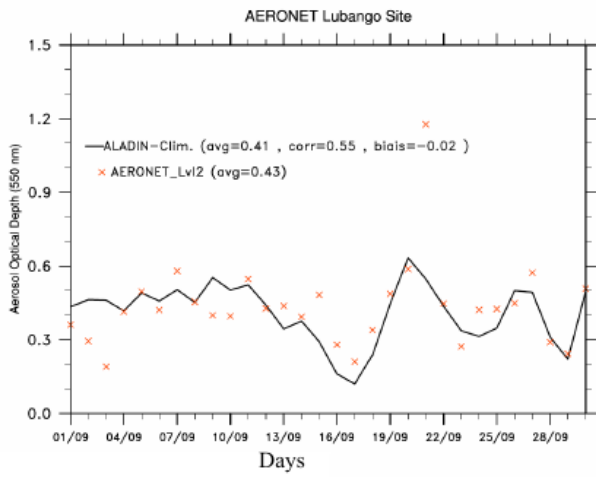


Figure 4. Total daily-mean AOD (at 550 nm) averaged over the box_S (5-15S / 15-25E) from the ALADIN-Climate model (10:30 and 13:30 UTC outputs are used), MERRA2 and derived from 2260 MODIS-Aqua DT data (left). Daily-mean ACAOD (at 550 nm) estimated from the MODIS-DB satellite and two different configurations of the ALADIN-Climate model (SMK and SMK_SN) averaged over the box_O (0-10N / 10-20E) (right). Uncertainties related to DT AOD and DB ACAOD are also indicated.

2265

2270

2275



2280 **Figure 5.** Comparisons of daily-mean total AOD obtained at the Lubango, Mongu and Ascension Island AERONET stations (daytime model outputs only) for September 2016.

2285

2290

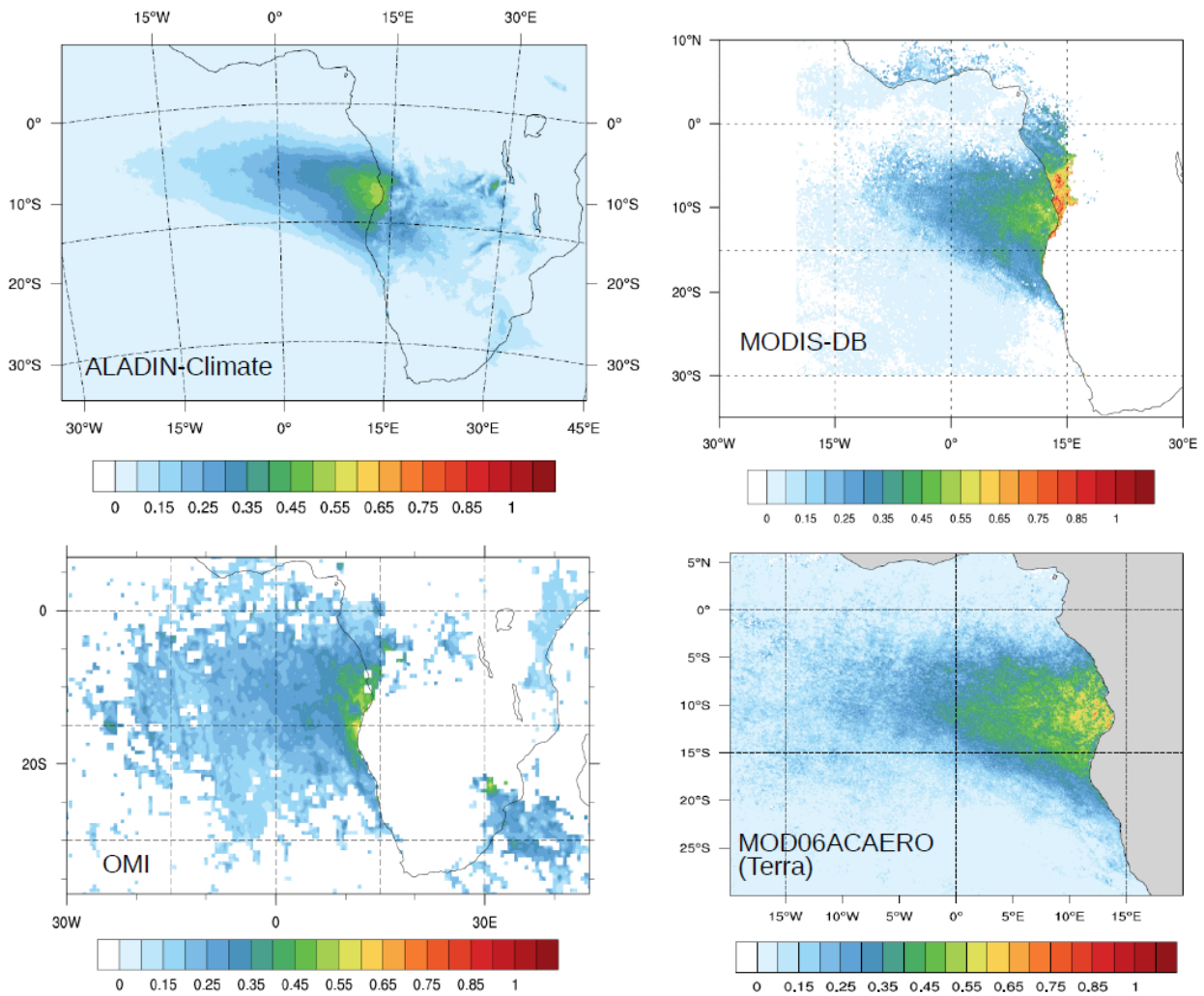


Figure 6 Total monthly-averaged ACAOD (at 550 nm) for September 2016 simulated by the 2295 ALADIN-Climate (10:30 and 13:30 UTC outputs only are used) model and derived from MODIS (Deep-Blue and Meyer retrievals) and OMI instruments.

2300

2305

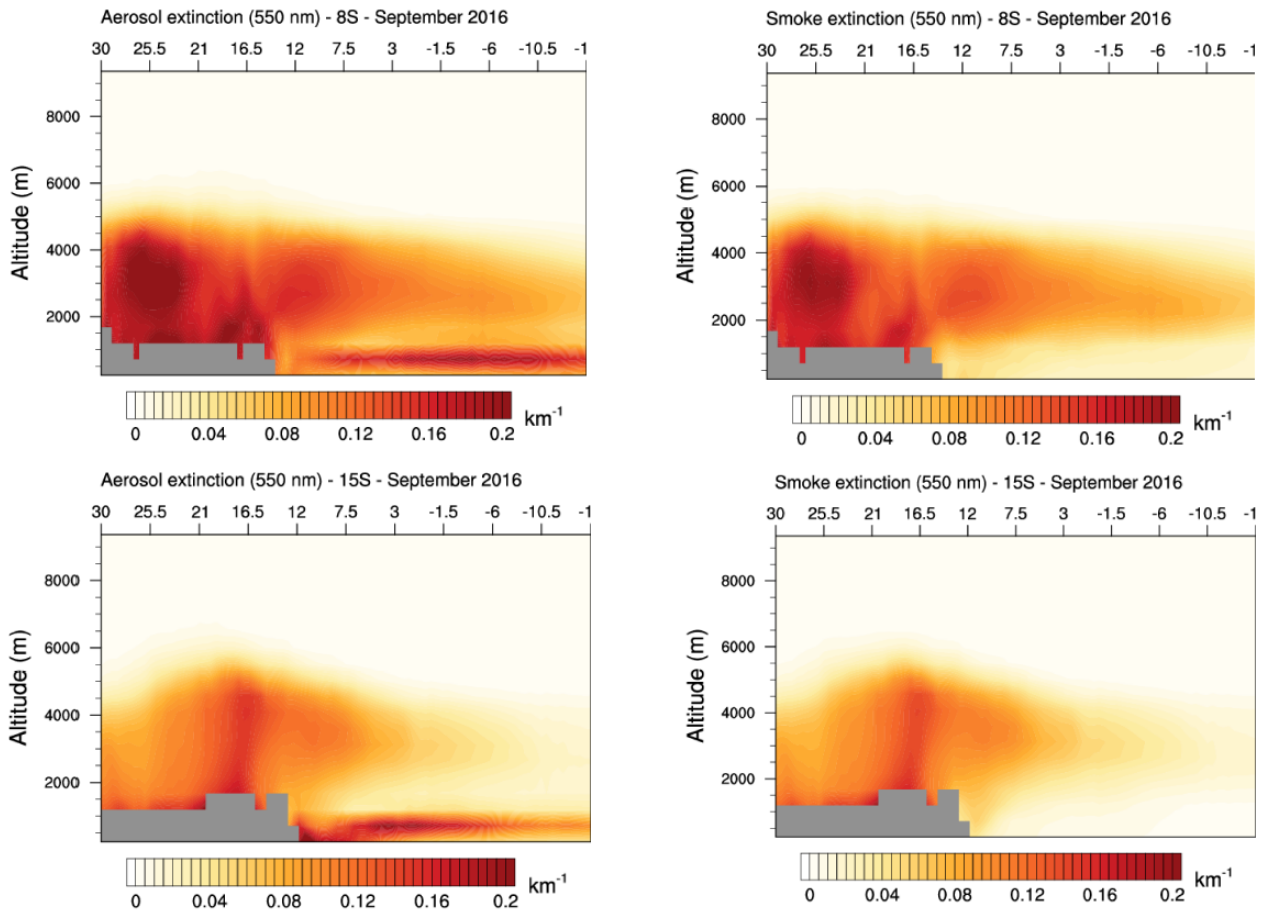


Figure 7. Monthly averaged vertical profiles of the total aerosol (left) and smoke (right) extinction coefficient (at 550 nm) simulated by the ALADIN-Climate model for two transects at latitudes of 8 and 15°S. Longitudes are between 30°E to 11.5°W.

2310

2315

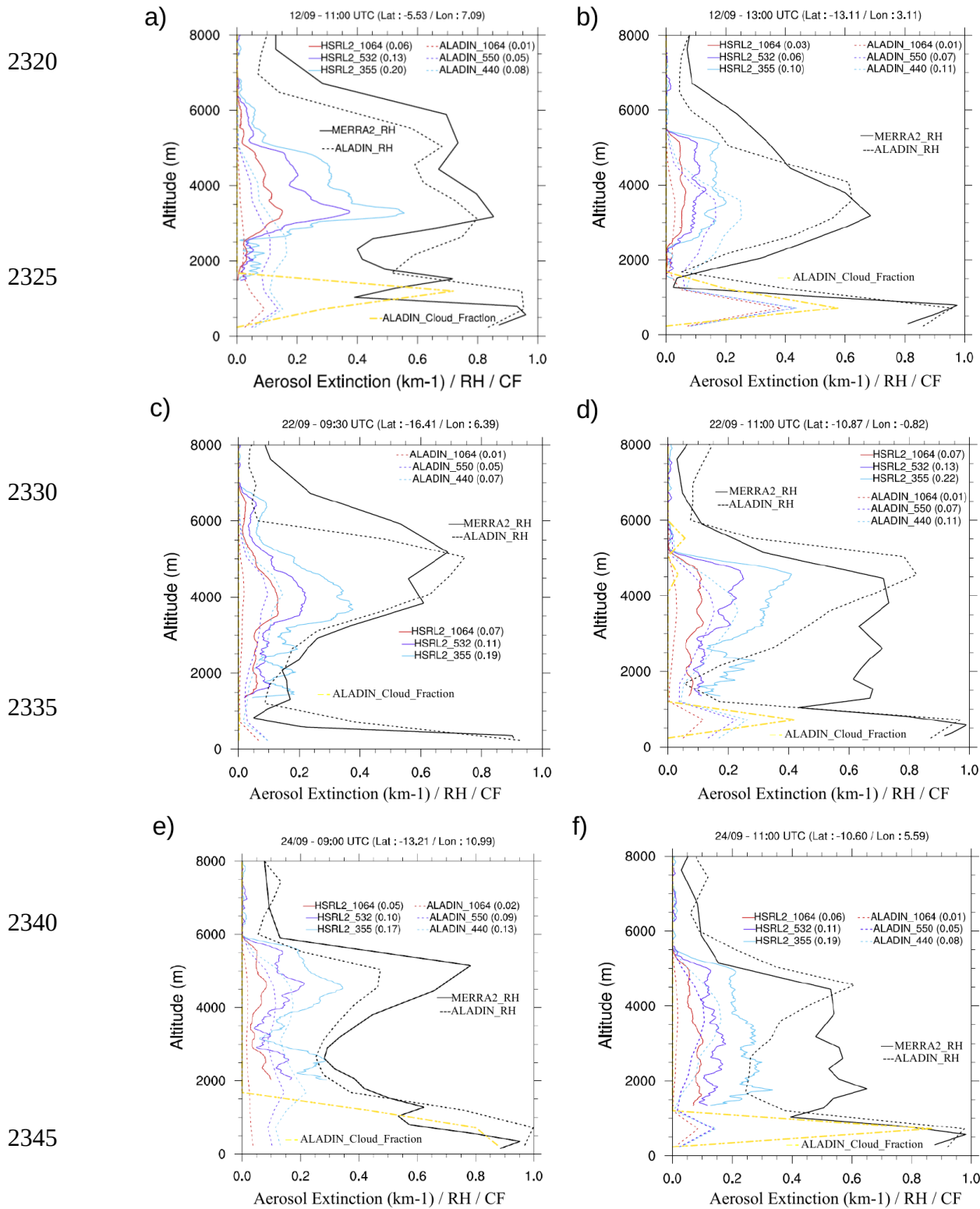
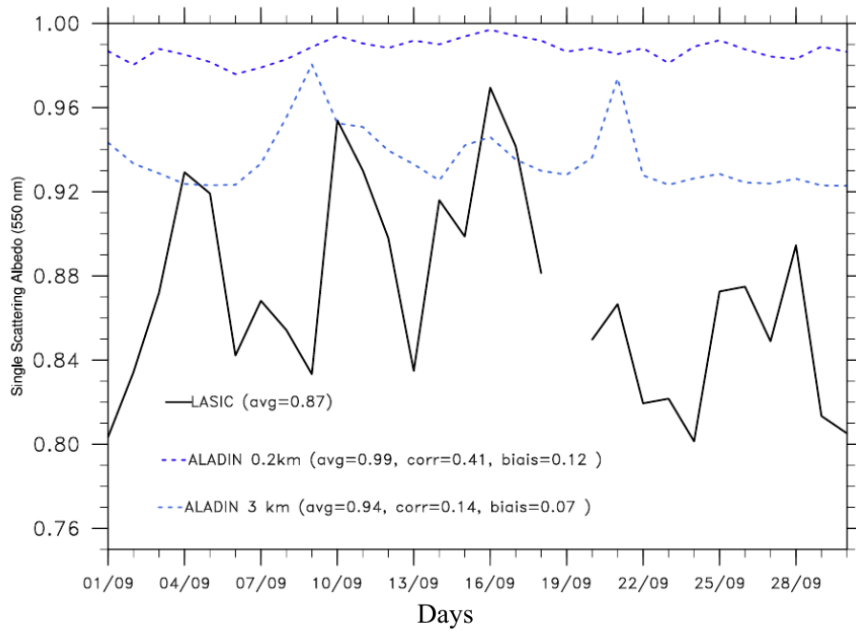


Figure 8. Vertical profiles of aerosol extinction coefficient (in km^{-1}) at three different wavelengths from ALADIN-Climate and HSRL-2 instrument (red: 1064 nm / purple: 550 nm / blue: 440 nm), associated with the mean values (note that the wavelengths are not exactly similar, especially in ultraviolet). Also reported are the vertical profiles of RH simulated by ALADIN-Climate (dotted black) and MERRA2 (black), as well as the ALADIN-Climate cloud fraction (dotted yellow).

2355



2365

Figure 9. Daily-mean in-situ SSA estimated at the surface at Ascension Island (LASIC) and simulated with the ALADIN-Climate model at two different altitudes (0.2 and 3 km).

2370

2375

2380

2385

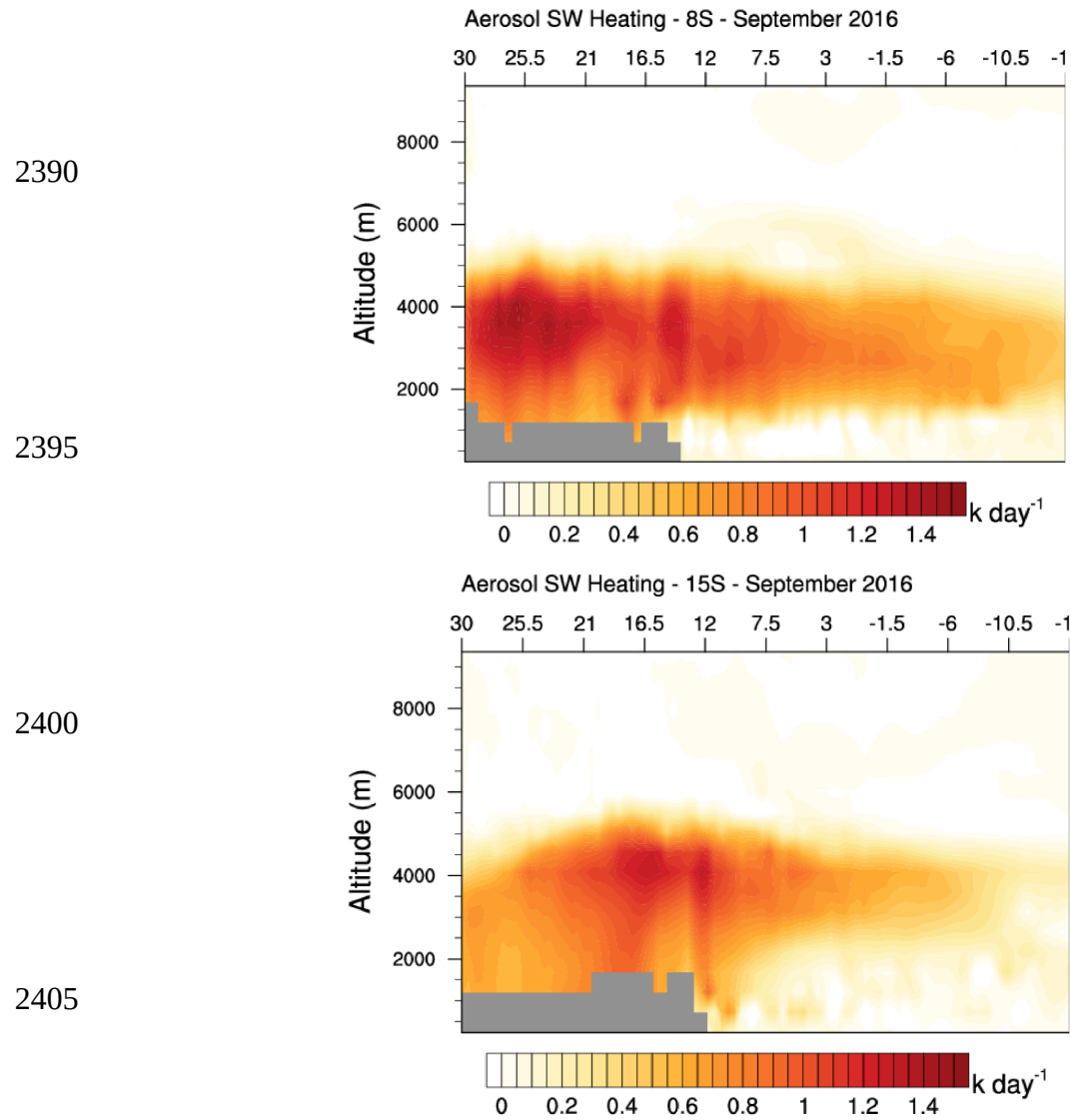


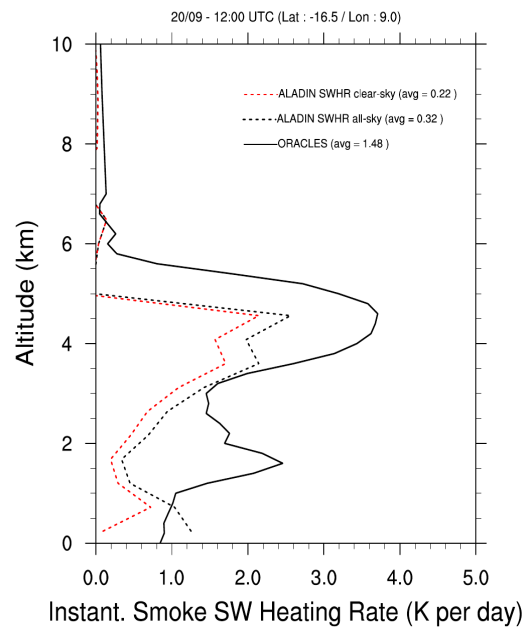
Figure 10. Monthly-mean (September 2016) aerosol SW heating rate vertical profiles simulated by the ALADIN-Climate model for two transects at latitudes of 8 (top) and 15°S (bottom). Longitudes are between 30°E to 11.5°W.

2415

2420

2425

2430



2435

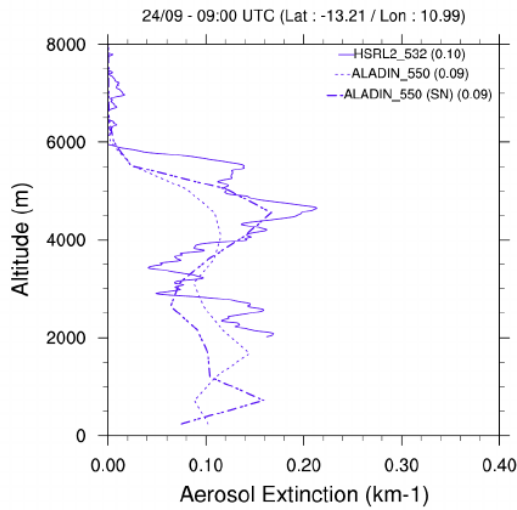
Figure 11. Instantaneous SW heating rate (12:00 UTC) only due to smoke aerosols, obtained from ORACLES aircraft data and simulated by the ALADIN-Climate model in clear-sky (red dashed) and all-sky (blue dashed) conditions.

2440

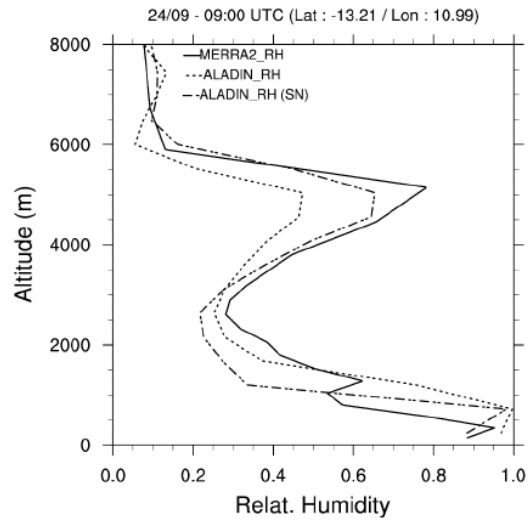
2445

2450

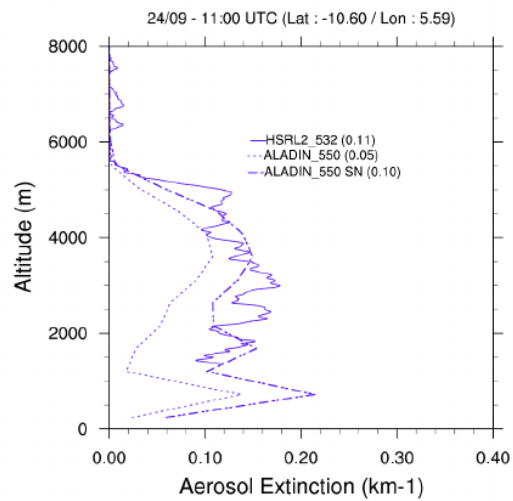
2455



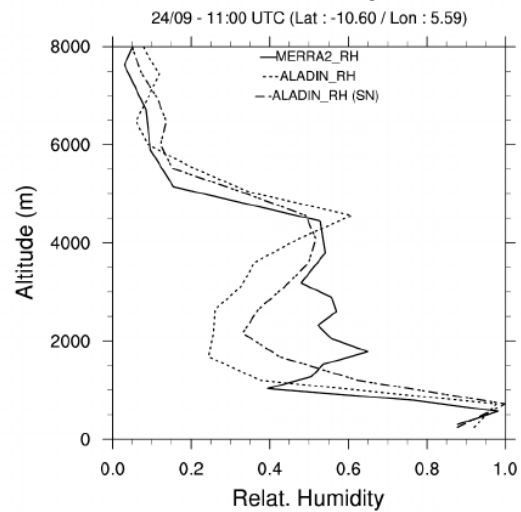
2460



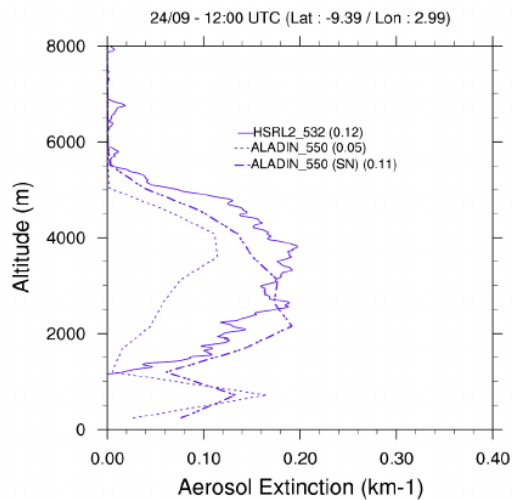
2465



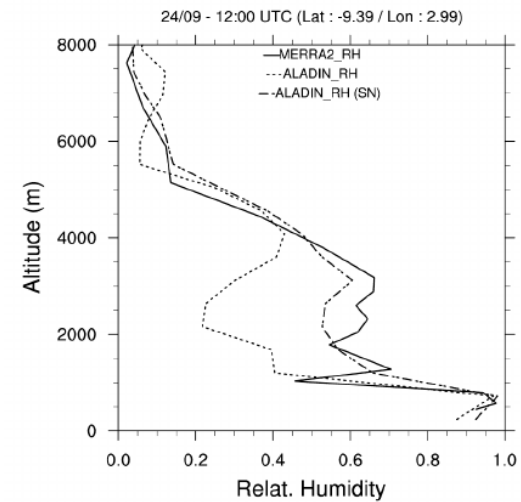
2470



2475



2480



2485 **Figure 12.** Vertical profiles of aerosol extinction coefficient (at 550 nm) obtained from ALADIN-Climate for the SMK and SMK_SN simulations, and derived from the HSRL-2 instrument for the 24/09, associated to the vertical mean (left panels). Also reported the RH obtained from the same simulations and MERRA2 data (right panels).

2490

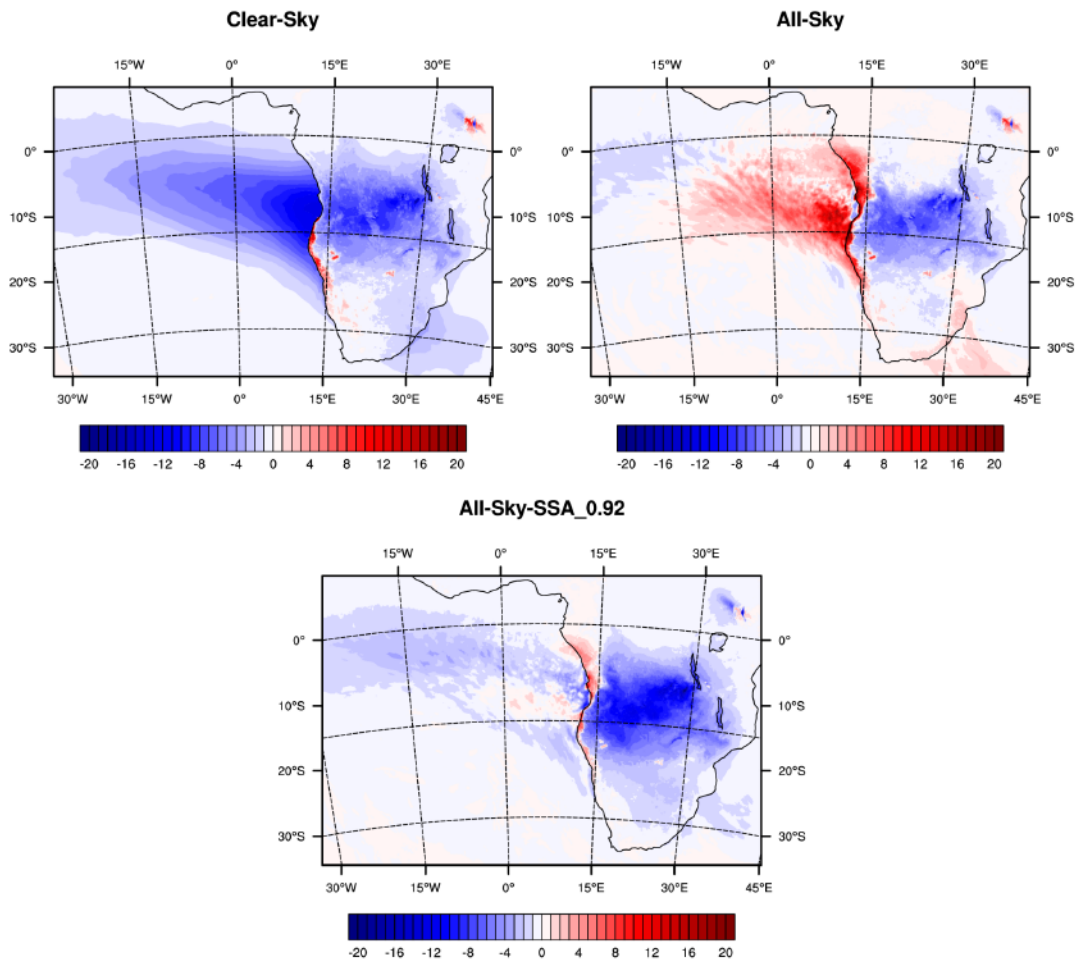
2495

2500

2505

2515

ALADIN-Climat Monthly-mean DRF (SW) at TOA - September 2016

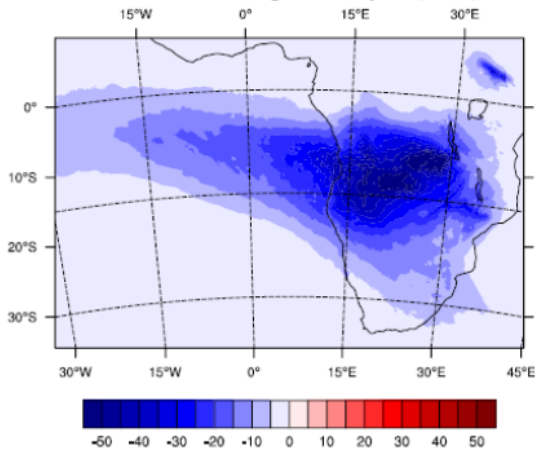


2510

Figure 13. Monthly-mean SW DRF (W.m⁻²) exerted by smoke particles at TOA for the September 2016 period in clear-sky (left up) and all-sky (right up) conditions for the SMK simulation and for the (bottom) SMK_SSA run.

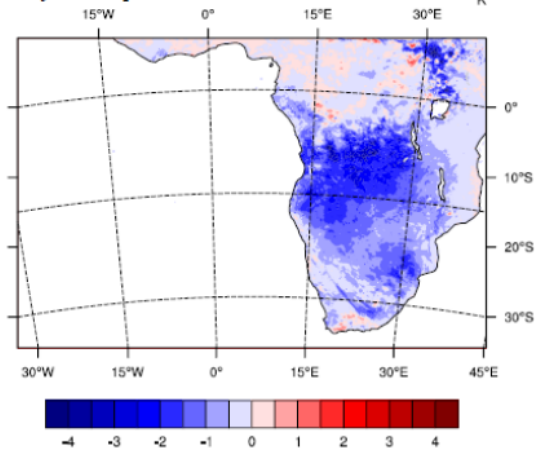
2520

Direct Radiative Forcing at the surface ($W.m^{-2}$)



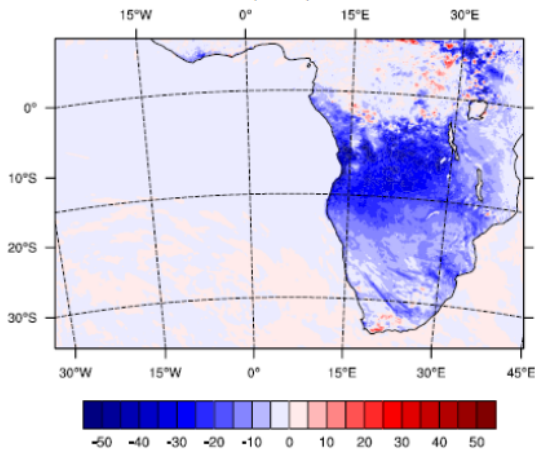
2525

Surface Temperature over land (K)



2530

Sensible Heat Fluxes ($W.m^{-2}$)



2535

PBL altitude (m)

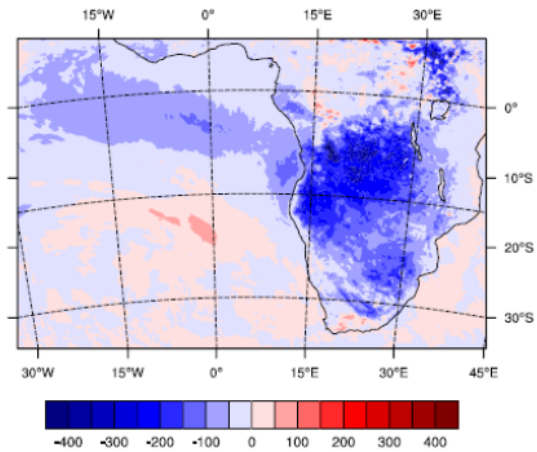
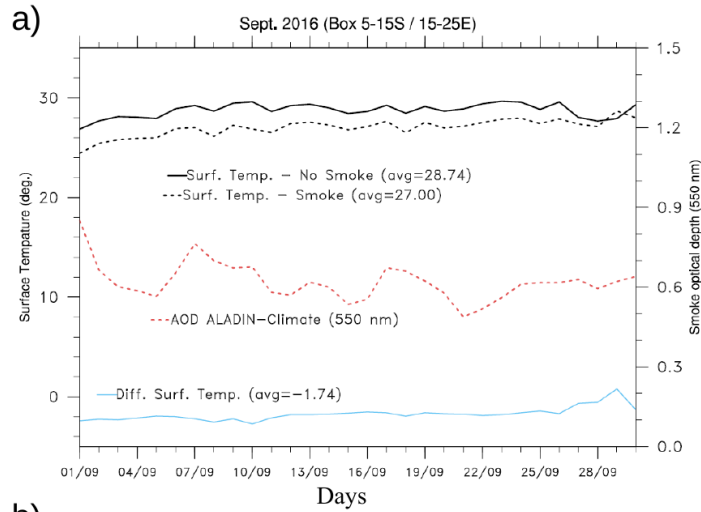


Figure 14. Differences between the CTL and SMK ALADIN-Climate runs in the monthly-mean (September 2016) SW surface radiations (top left), 2 meter continental temperature (top right), sensible heat fluxes (bottom left) and PBL height (bottom right).

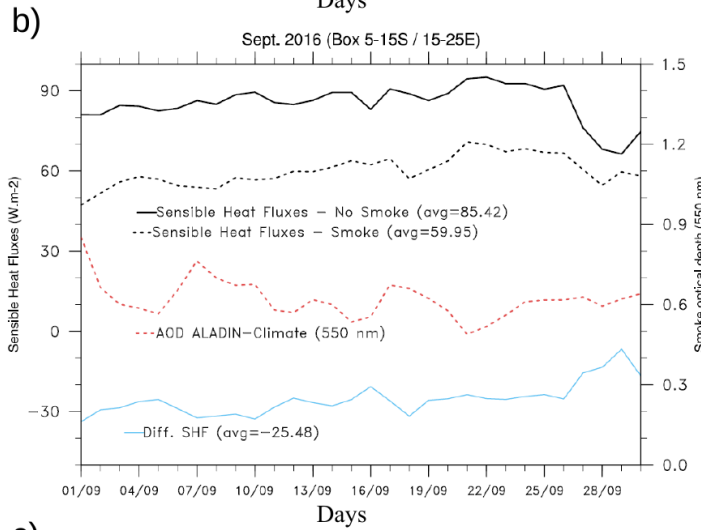
2540

2545

2550

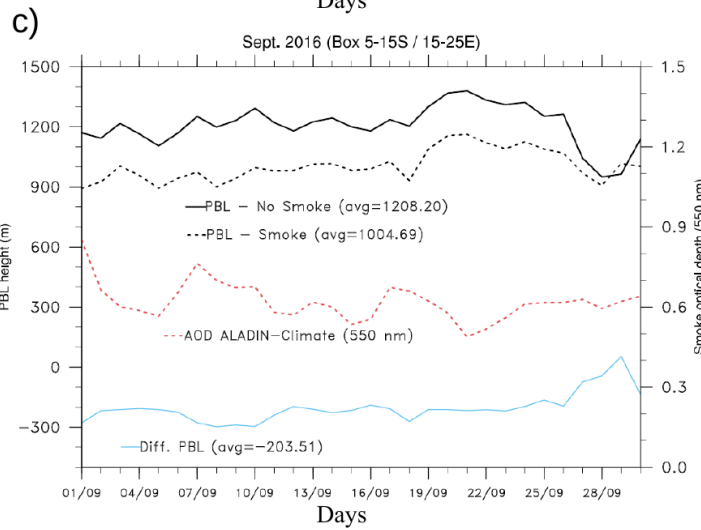


2555



2560

2565



2570

2575

Figure 15. Daily-mean Surface Temperature, Sensible Heat Fluxes and PBL height obtained from the CTL (black lines) and SMK (dashed black) ALADIN-Climate simulations for september 2016. The AOD (red dashed lines) and the difference between the two simulations (CTL and SMK) for each variables are also reported (blue lines).